AN ABSTRACT OF THE DISSERTATION OF

Mahabub Alam for the degree of Doctor of Philosophy in Mechanical Engineering presented on September 16, 2016.

Title: Crack Penetration and Deflection Behavior at Interfaces

Abstract approved: _____

John P. Parmigiani

This study computationally and experimentally examines the mechanisms of crack penetration, deflection and the transition between penetration and deflection. The finite element analysis based computational modeling work used strength-and-energy based cohesive-zone approach to study the effect of dimensionless parameters (e.g., interfacial incident angle, fracture-length scale, and normalized toughness) on penetration/deflection behavior for mode-I loading (tensile load normal to crack plane). The first modeling work examines the effect of incident angle between crack plane and interface for a crack incident on an interface. As expected, results exhibit that small incident angles cause deflection whereas penetration is more likely at large incident angles. The transition between penetration and deflection becomes more strength-ratio dependent as incident angle decreases. It appears that, facture-length scale is an influential parameter in crack deflection criterion and chances of deflection reduces as fracture-length-scale decreases. Finally, the analysis looked at the effect of normalized-toughness and found that the normalized-toughness has a small effect on deflection criteria.

The second modeling work investigated the transition mechanism between deflection and penetration. The situation when both mode-I and mode-II works simultaneously is called mixed-mode, which is presented by the parameter phase angle. Phase angle 0° represents pure mode-I,

90° represents pure mode-II (shear load parallel to crack plane), and any phase angle in-between 0° and 90° represents mixed-mode. Results have shown the presence of smaller phase angle in the crack-tip at transition than deflection, while the applied load is elevated at transition due to providing the required energy for both the penetration and deflection. The difference of phase angles between transition and deflection becomes low as fracture-length-scale decreases. The results of cohesive-zone model meet Linear Elastic Fracture Mechanics (LEFM) results for the case of small fracture-length scales. This work analyzed interfacial phase angle during transition, between penetration and deflection, not only for homogeneous materials system but also for modulus mismatch. It was found that stiffer first-phase materials tend to create higher phase angle at the crack tip interfaces; the cases for low modulus mismatches are more sensitive than high modulus mismatches.

A systematic experimental study was performed to compare results with the cohesive-zone method, LEFM, and strength-based method results. A brittle polymer Polymethyl methacrylate (PMMA) was used as substrate material, and two different kind of solvent adhesives Weld-On 4 and Weld-On 16 were used as interfaces that have similar elastic modulus as PMMA. The interfaces created by Weld-On 4 are weaker while Weld-On 16 creates stronger interfaces; however, they have similar toughness. Crack incident angle varied from 75° to 90° with 5° increment. Critical incident angle at transition between penetration and deflection was investigated for each type of interfaces. The results showed that cohesive-zone method can predict crack deflection better than energy-based LEFM; material-to-interface toughness-ratio and strength-ratio both have influence on the transition event.

Copyright by Mahabub Alam
September 16, 2016
All Rights Reserved

Crack Penetration and Deflection Behavior at Interfaces

by
Mahabub Alam

A DISSERTATION

submitted to

Oregon State University

in partial fulfillment of
the requirements for the
degree of

Doctor of Philosophy

Presented September 16, 2016
Commencement June 2017

Doctor of Philosophy dissertation of Mahabub Alam presented on September 16, 2016

APPROVED:

Major Professor, representing Mechanical Engineering

Head of the School of Mechanical, Industrial, and Manufacturing Engineering

Dean of the Graduate School

I understand that my dissertation will become part of the permanent collection of Oregon State University libraries. My signature below authorizes release of my dissertation to any reader upon request.

Mahabub Alam, Author

ACKNOWLEDGEMENTS

It is my pleasure to thank many people for whom this dissertation was possible.

First of all, I would like to acknowledge and thank my Ph.D. supervisor, John Parmigiani. He made me a mechanical engineer and researcher. He pushed when required to keep me on track with a reasonable pace. Of course I would like to thank my Ph.D. co-supervisor, Jamie Kruzic, who taught me how to design, and perform experiments. I also learned experimental research ethics from him.

I am indebted to my student colleagues in professor Parmigiani group and professor Kruzic group for their support and patiently answering my relevant and irrelevant questions. As for the local community, I would like to thank my friends in Corvallis, for helping me get through the difficult times, and for all the emotional support, entertainment, and caring they provided.

Primarily my wife, Farah Naz Efa, who supported me without any question, showed me the up peak while I am in the down peak of my doctoral roller coaster. This achievement was not possible without her. Especially, I would like to thank my parents, Abdul Matin Sarker and Lili Akhter. They raised me, encouraged me, supported me, taught me, loved me, and sacrificed a lot for me. Also, I wish to thank my sister, Kamrunnahar Lima, who is my all-time mentor and best friend. I wish to thank my entire extended family for providing a loving environment for me.

Finally, thanks to everyone who I can't remember to add to this list.

CONTRIBUTION OF AUTHORS

Dr. John Parmigiani was involved in advising and providing feedback for Chapter 2, and 3. Dr. Jamie Kruzic was involved in advising and providing feedback for Chapter 4.

TABLE OF CONTENTS

Page

TABLE OF CONTENTS (Continued)

Page

LIST OF FIGURES

Page

LIST OF FIGURES (Continued)

Page

LIST OF FIGURES (Continued)

Page

LIST OF TABLES

Table Page

Chapter 1 : General Introduction

Understanding crack propagation behavior at an interface is a key aspect of composite materials design. Consider, for example, an interface created by joining two layered materials; a through crack present in the first material incident on the interface, may penetrate to the second material, or may deflect along the interface. Crack penetration/deflection at interfaces is a very important event for strength and toughness properties of many composite material systems. Interfaces are present in many engineering applications including fiber reinforced polymers, toughened ceramics, laminated composites, and microelectronic packages. A fiber reinforced composite is usually tougher than its own matrix, provided cracks deflect at the interfaces. If a crack grows through matrix, hindered by an interface between fiber and matrix, then continues along the interface, the intact fiber creates crack bridging. On the contrary, the bridging was not possible if the crack would continuously grow through the fiber without being hindered by the interface. The strength or toughness of a composite does not improve significantly if the fiber has similar material properties as the matrix and promotes penetration through the interfaces [1]. Layered materials combining brittle and ductile layers exhibit more fracture resistance due to renucleation of cracks, interfacial debonding, and slipping at interfaces [2]. In the similar way, crack bridging whiskers or particles increase high fracture resistance for toughened ceramics [3, 4]. A signification amount of energy dissipation occurs due to the debonding of fiber-matrix interfaces, and frictional resistance of the fractured planes along the interfaces [5, 6]. Crack deflection along interfaces may increase the toughness property of materials by debonding interfaces, energy dissipation due to friction, and crack bridging mechanism.

Many natural composites (e.g., wood, oyster shell, bones, etc.) provide high toughness that depends on the crack deflection mechanism [7-9]. For example, wood contains longitudinal fibers and exhibits high fracture resistance when the crack is incident normally to the fibers [10]. Oyster shell and shells of many animals are tough due to the mixture of different materials including protein and minerals. Protein creates the adhesive bonds between mineral layers, which debonds and absorbs energy to make the shell tough [7, 9, 11]. Bone consists of mineral crystals embedded in an organic matrix of protein collagen. If an attempt is being made to fracture bone, the bonding agent protein delaminates and dissipates energy. For designing a better bone implant, it is important to make sure chosen materials provide a similar deflection mechanism to give mechanical properties similar to bone [12]. Similar is true for designing artificial wood-plastic composites, or dental implants.

While much research has considered normal cracks incident on interfaces, less focus has been given to the effect of incident angles. In nature, crack may incident at an interface in many angles rather than maintaining a 90° incident angle. A crack within a grain of a material may create any angles with a grain boundary. Some applications require an understanding of the incident angle of penetration versus deflection behavior, for example the indentation of interface fracture (IIF) test for measuring the relative toughness of an interface [13]. Foulk III et *al.* [14] showed penetration versus deflection behavior is a strong function of incident angle for a high-strength and low-toughness material system. The combined effect of strength, toughness, and incident angle on crack penetration/deflection behavior for a wider range of material systems are much less understood.

When prediction of crack deflection is necessary for designing composite materials, a few approaches are available. Listed here earlier to newer, the strength-based approach, energy-based approach, and strength-and-energy based approach (also known as cohesive-zone model) are available to predict deflection at interfaces. Strength-based approaches use the Inglis approach [15] for fracture propagation. According to this approach, applied stress has to exceed the cohesive strength of materials for a crack to propagate. Gupta *et al.* [16] first developed a strength based deflection criterion for a crack normally incident on an interface of a bi-material system. Deriving their analysis for a homogeneous system, a crack should deflect for a substrate three and half times stronger than the interface. Although the strength-based methods have limitations, they are still used by many people for computational efficiency in modeling multi-crack-deflection. Another approach, the energy-based approach, has been heavily used for last three decades for brittle material system [17-19]. The energy-based approach is based on the Griffith approach [20] to fracture, assuming linear elasticity and an existing flaw at an interface. Implementing Linear Elastic Fracture Mechanics(LEFM), He and Hutchinson [17] predicted crack deflection for a substrate material four times tougher than interface, considering a normally incident crack of a homogeneous material system. While the strength-based approach only considers the strength of materials, the energy-based approach focuses solely on the toughness of materials, with a presumption that the strength criterion is already satisfied because of the singularity at the crack tip of linear elastic materials. The criteria solely based on linear elastic material properties may not be applicable for many practical applications for which stress across the interface is limited in magnitude. Some research exhibited that the recent strength-and-energy based approach cohesive-zone method is applicable for a wider range of materials rather than linear elastic materials[21-24].

The cohesive-zone method uses traction-separation law that naturally incorporates both strength and toughness parameters as crack propagation criterion. In this method the bonding mechanism at interfaces of composites can be considered by traction (or stress) as a function of separation. A traction-separation law can be utilized to characterize bonding. Traction increases with separation until it reaches to the strength of material, and traction decreases to zero for a critical separation to failure. In other words, a fracture to occur, applied stress has to satisfy the cohesive strength of the material (peak of a traction-separation law) and supplied energy has to overcome the fracture toughness (total area under the traction-separation law) of the material. Traction can be formed by cohesive or adhesive bonding of engineered, physical, or biological materials. The size and shape of the traction-separation law depends on the properties of material and geometrical parameters [25]. While much has been discovered about the applicability of cohesive-zone method for explaining penetration versus deflection event, there are still opportunities for exploring the full potential of the method. Accordingly, this dissertation will examine the effects of incident angles along with length of plastic zone at crack tip and normalized toughness on crack penetration/deflection behavior.

Since several approaches available to predict crack deflection, the next logical key question for a user would be, which approaches can best predict natural crack penetration/deflection? To answer this question, an experimental study is required to compare predictions from individual approaches with experimental observations. There are some experimental studies to test the energy based approach for predicting penetration/deflection for dynamic loading [26, 27]. To authors' knowledge, there is no existence of work to test the accuracy of the prediction of crack deflection by different existing approaches for static or quasi-static loading. Accordingly, this dissertation

will experimentally examine the predictability of crack deflection by strength-based, energy-based and strength-and-energy based cohesive-zone model.

The study conducted in this doctoral dissertation is comprised of three manuscripts as Chapter-2 to Chapter-4: i) Effect of Incident Angle on Crack Propagation at Interfaces, ii) Crack-Tip Interface Phase Angle for Mode-I Remote Loading, and iii) An Experimental Assessment of Models to Predict Crack Deflection at an Interface. The first two studies are based on finite element modeling. The modeling part of this study used cohesive-zone method to evaluate the effect of parameters on the deflection criteria and examined the mechanism of transition between penetration and deflection. The experimental part correlated and compared the correctness of the deflection criteria of stress-based methods, energy-based methods, and cohesive-zone method with the experimental observation.

The first modeling study assessed the effect of incident angle parameter on crack deflection criterion for mode-I quasi-static loading. Trapezoidal traction-laws have been used as material properties; different size and aspect ratio of the trapezoid represents different material's properties. Dimensionless parameters used for a generalized use of a range of material systems. The effect of fracture-length scale and normalized-toughness were assessed in this study. The strong dependency of crack penetration/deflection with strength and toughness properties of materials and interfaces along with incident angle geometric properties is exhibited in this study.

The second modeling study, used similar cohesive-zone model and geometry as the first study, examines the mechanisms of interfacial crack at transition between penetration and deflection. The magnitude of phase angle represents the mixed mode stress state at interfaces. Fracture-length scale and normalized-toughness were systematically varied to investigate their

effect on the transition event. The effect of modulus mismatch also has been examined and found a strong influence on crack deflection.

The experimental study evaluated different existing methods as crack deflection criteria: cohesive-zone method, energy-based method LEFM, and strength-based method. A brittle polymer PMMA and solvent type nearly-zero thickness interfaces were used to assess the effect of energy and strength parameters. It has shown that cohesive-zone method predicts better than energy-based LEFM. As expected, the analysis shown that the chances of deflection enhance as incident angle decreases. In this study, incident angle varied to get the critical incident angle at transition for each material system. Results of this study provide insight into the dependency of crack deflection on strength, energy and incident angle.

Chapter 2 : Effect of incident angle on crack propagation at interfaces

2.1 Introduction

The load carrying ability of a composite is significantly affected by the manner in which a crack propagates when encountering an interface between constituent materials. Propagation occurring by deflection (i.e. growth along the interface) tends to blunt the crack tip and increase macroscopic toughness. Propagation occurring by penetration (i.e. growth across the interface) tends to the opposite. Whether deflection or penetration occurs depends on a number of factors such as the material properties of the constituent materials and interfaces. Strong, tough constituent materials will tend to promote deflection and strong, tough interfaces will tend to promote penetration. Also of significance is the crack geometry, particularly the incident angle between the crack and the interface. Small angles promote deflection and large angles promote penetration. An application of the dependence on both material properties and incident angle of deflection versus penetration behavior is the indentation interface fracture (IIF) test which is used to measure the relative toughness of a bonded interface[13]. Despite the significance of incident angle, much of the research on penetration versus deflection behavior has not included its effect.

A large body of literature exists related to crack propagation by deflection versus propagation and criteria for predicting transition from one to the other. The earliest published work, written over 50 years ago, is that of Cook et *al.* [28]. They used a simple stress-based criterion to predict if deflection would occur. Subsequently, others pursued more sophisticated stress-based approaches to determine transition criteria [16]. Also a number of others have used

energy-based, or LEFM, approaches [19, 29-31]. Some of this work included a discussion of the effect of incident angle [17]. However, more recently it has been shown that a combined stress-and-energy-based approach is necessary, particularly regarding the transition between deflection and penetration [21, 32, 33]. It has been shown that the energy-based approach is a special case of the more general combined stress-and-energy-based solution [23]. The stress-and-energy-based approach has been used to explore the effect of incident angle for a high-strength, low-toughness material system [14]. For this material system it was found that the propagation by deflection versus penetration was a strong function of incident angle. However, a study using the combined stress-and-energy-based approach and spanning a wider range of material systems to explore the effect of incident angle on crack propagation by deflection versus penetration does not currently exist in the literature.

This paper presents work using the cohesive-zone approach of Parmigiani and Thouless [21]. The study of the effect of incident angle on the transition between propagation by deflection and penetration is extended in several significant aspects: results are given for incident angles of zero to ninety degrees in terms of dimensionless groups, key results are compared to LEFM special-case solutions, and insight is provided on why data trends occur. Also the effect of an additional dimensionless group, not explicitly considered in prior work, is explored.

2.2. Methods

2.2.1 Cohesive zone model

The cohesive zone approach used in this paper is based on the work by Thouless [34-36]. It consists of two separate trapezoidal traction laws joined by a failure criterion. One traction law, illustrated in Figure 2-1a, gives crack-tip normal stress as a function of the normal

displacement in the crack-tip process zone. The maximum stress given by this traction law, denoted by $\hat{\sigma}$, is the cohesive normal strength. The maximum normal displacement given by this traction law, denoted by δ_{n3}, is the critical normal displacement corresponding to fracture for pure mode I loading. Similarly, a second traction law, illustrated in Figure 2-1b, gives crack-tip shear stress as a function of the shear displacement in the crack-tip process zone. The maximum stress ($\hat{\tau}$) is the cohesive shear strength and the maximum displacement (δ_{s3}) is the critical shear displacement that corresponds to fracture for pure mode II loading. The total area under normal traction law and under the shear traction law (i.e. the areas of the trapezoids) equals the mode I fracture toughness and mode II fracture toughness respectively. The partial areas under each traction law corresponding to displacements greater than zero and less than the critical values equal the instantaneous energy release rates denoted as G_I and G_{II} respectively for the normal and shear cases. Pure mode I loading uses the normal traction law exclusively and pure mode II loading uses the shear traction law exclusively. Mixed-mode loading requires the use of both laws. A simple linear combination of the mode I and mode II energy-release-rate to toughness ratios is used and is given by

$$\frac{G_I}{\Gamma_I} + \frac{G_{II}}{\Gamma_{II}} = 1 \tag{2.1}$$

2.2.2 Finite element model

The model used in this study, illustrated in Figure 2-2, consists of two semi-circular sections bonded at a diametral interface to form a disk. A radial crack of length R, extending from the disk circumference to the disk center and incident on the interface at an angle ϕ, is present in one of the sections. Each section is comprised of the same homogeneous isotropic

material. Pure plane-strain mode I loading was applied to the crack through the application of displacement boundary conditions at the disk circumference. These boundary conditions were calculated from the LEFM relationships for displacement under plane strain conditions given by

$$u_x = \frac{K_I(1+v)}{E}\sqrt{\frac{R}{2\pi}}cos\left(\frac{\theta}{2}\right)\left[2-4v\ +2\,sin^2\left(\frac{\theta}{2}\right)\right] \tag{2.2}$$

$$u_y = \frac{K_I(1+v)}{E}\sqrt{\frac{R}{2\pi}}sin\left(\frac{\theta}{2}\right)\left[4-4v+2\,cos^2\left(\frac{\theta}{2}\right)\right] \tag{2.3}$$

Where the x and y axes have origin at the disk center and are aligned with the crack and horizontally to the right respectively, K_I is the mode I stress intensity factor, v is Poisson's ratio, E is Young's modulus, r is the radial distance from the disk center, and θ is an angle measured counterclockwise from the positive x-axis.

The finite element analysis was performed using the commercial package Abaqus (version 6.13). The traction laws and failure criterion were implemented as cohesive-zone elements in a FORTRAN subroutine using a user element (UEL). The subroutine used is similar to that used by Parmigiani [4]. The cohesive-zone elements were placed in the mesh wherever crack propagation could occur. Since the crack is subjected to mode I loading, propagation could occur in two ways. The first, referred to as penetration, is propagation across in interface and in the same direction as the crack. The second, referred to as deflection, is to turn and propagate along the interface. These two possibilities required that cohesive zone elements be placed radially vertically downward and also be placed along the interface. Elsewhere Abaqus 2-D plane strain continuum elements (CPE4R) were used. The total number of elements in this model is 48,390. A mesh convergence study was performed to determine suitable element size.

Element size varies with the smallest being located near the crack tip and the largest at the periphery. The element size is very small at the crack tip. The ratio of the size of the smallest element to the length of the crack, R, is 9×10^{-6}.

2.2.4 Material properties and geometric parameters

The relevant parameters controlling the propagation, by either penetration or deflection, of the crack in the model of this study are as follows.

$$\Gamma_m, \Gamma_{Ii}, \Gamma_{IIi}, \hat{\sigma}_m, \hat{\sigma}_i, \hat{\tau}_i, \bar{E}, \nu, R, \phi$$

Where Γ_m is the mode I toughness of the material comprising the semi-circular sections, Γ_{Ii} is the mode I toughness of the interface, Γ_{IIi} is the mode II toughness of the interface, $\hat{\sigma}_m$ is the mode I strength of the material comprising the semi-circular sections, $\hat{\sigma}_i$ is the mode I strength of the interface, $\hat{\tau}_i$ is the mode II strength of the interface, $\bar{E}$ is Young's modulus under plane strain conditions (i.e. $E / 1-\nu^2$) of the material comprising the semi-circular sections, and ν, R and ϕ are as previously defined. These parameters are more effectively written in terms of the following dimensionless groups.

$$\phi, \frac{\hat{\sigma}_i}{\hat{\tau}_i}, \frac{\Gamma_{IIi}}{\Gamma_{Ii}}, \frac{\hat{\sigma}_m}{\hat{\sigma}_i}, \frac{\Gamma_m}{\Gamma_i}, \frac{\Gamma_m}{\bar{E}R}, \frac{\bar{E}\Gamma_i}{\hat{\sigma}_i^2 R}$$

Where ϕ was varied from 0° to 90°, $\hat{\sigma}_i/\hat{\tau}_i$ was held constant at a value of one, and $\Gamma_{IIi} / \Gamma_{Ii}$ was also held constant at a value of one. The parameter Γ_i denotes the common value of interface toughness (i.e. $\Gamma_i = \Gamma_{IIi} = \Gamma_{Ii}$). The effects of the remaining four groups on penetration versus deflection behavior are explored in subsequent sections. Poisson's ratio was kept constant at a value of 0.3. Without a loss of generality, the groups $\Gamma_i/\bar{E}R$ and $\bar{E}\Gamma_m/\hat{\sigma}_m^2 R$ can be used in place

of groups $\Gamma_m/\bar{E}R$ and $\bar{E}\Gamma_i/\hat{\sigma}_i^2 R$. For some of the results presented in this paper, $\bar{E}\Gamma_i/\hat{\sigma}_i^2 R = \bar{E}\Gamma_m/\hat{\sigma}_m^2 R$ in order to simplify the discussion of key concepts. However, the results presented are generally applicable to cases of $\bar{E}\Gamma_i/\hat{\sigma}_i^2 R \neq \bar{E}\Gamma_m/\hat{\sigma}_m^2 R$.

Examples of the values of these parameters can be obtained from the literature. For transgranular (penetration) versus intergranular (deflection) fracture of Silicon Nitride, values are $\hat{\sigma}_i/\hat{\tau}_i \sim 3.0$, $\Gamma_m / \Gamma_I \sim 5.5$, $\Gamma_m/\bar{E}R \sim 1.5 \times 10^{-5}$, and $\bar{E}\Gamma_m/\hat{\sigma}_m^2 R \sim 0.001$ [14]. For a thermosetting polyester (Homalite H-100) and a structural adhesive (Weldon-10), values are $\hat{\sigma}_i/\hat{\tau}_i \sim 6.2$, $\Gamma_m / \Gamma_I \sim 0.62$, $\Gamma_m/\bar{E}R \sim 2.5 \times 10^{-7}$, and $\bar{E}\Gamma_m/\hat{\sigma}_m^2 R \sim 0.002$ for a 100 mm crack [26, 27, 37].

The displacement parameters defining the shape of the traction laws (δ_{n1}, δ_{n2}, δ_{n3}, δ_{s1}, δ_{s2}, and δ_{s3}) can also be written in dimensionless form as δ_{n1}/δ_{n3}, δ_{n2}/δ_{n3}, δ_{s1}/δ_{s3}, and δ_{s2}/δ_{s3}. However, variation in the values of these groups does not have a significant effect on results. They were held fixed at values of 0.05, 0.90, 0.05, and 0.90 respectively.

The dimensionless group $\bar{E}\,\Gamma/\hat{\sigma}^2 R$, referred to as the fracture length scale, has an important physical interpretation. As fracture length scale magnitude increases so does the length of the process zone). If the instantaneous energy release rate is used in place of the toughness, a comparison of magnitudes of this dimensionless group can be used to determine the relative sizes of the penetrating and deflecting crack-tip process zones [23]. Furthermore, small magnitudes of the fracture-length scale indicate a correspondence to the conditions required for linear elastic fracture mechanics (LEFM) to be valid. This can be shown by recalling that a common criterion for the use of LEFM with metals is that the size of the region of plasticity at the crack tip must be small compared to the crack length and other geometric dimensions of the object containing the

crack. Using the crack-tip stress-field equations derived from linear elasticity and the material's yield strength this criterion is often written as

$$\left(\frac{K_I}{\sigma_y}\right)^2 \ll L_c \tag{4}$$

where K_I is the stress intensity factor, σ_y is the metal's yield strength, and L_c is a characteristic length equal to the shortest distance from the crack tip to the boundary of the cracked object [38]. This criterion can be translated to apply to cohesive-zone fracture by substituting the product of Young's modulus and fracture toughness for the square of the stress intensity factor, substituting the cohesive strength for the yield strength, substituting the length of the un-cracked ligament (i.e. the radius of the disk) for the characteristic length, and rearranging to give

$$\frac{E\,\Gamma}{\hat{\sigma}^2\,R} \ll 1 \tag{2.5}$$

Given this, one would expect that, if other conditions are suitable, small values of fracture-length scale would correspond to LEFM conditions. An example of this behavior is illustrated in Figure 2-3 where it is shown that a K-field exists at the crack tip at small $\bar{E}\,\Gamma/\hat{\sigma}^2 R$ values. Also given in this figure are values of the length of the crack-tip process zone normalized by the radius R. Here the process zone has been defined as extending from the tip of the open crack to the location corresponding to the beginning of the horizontal section of the traction law. Other examples, from prior work, show that at small fracture-length scales the applied load required for crack propagation agrees with LEFM predictions [22, 23].

2.3 Results

The effect of incident angle on penetration versus deflection behavior was investigated for $\bar{E}\ \Gamma_i/\hat{\sigma}_i^2 R = 0.01$ and $\Gamma_m/ER = 10^{-6}$. Results are shown in Figure 2-4. In this figure, the solid lines indicate the transition between crack propagation by penetration and crack propagation by deflection at the indicated incident angle (i.e. penetration occurs in the region to the left of each solid line and deflection to the right). The horizontal and vertical axes are the ratios of material-to-interface strength and toughness respectively. The circular markers indicate calculated data points. Dashed lines correspond to constant values of the material fracture length scale. Results are consistent with prior work, done at an incident angle of 90° and using a rectangular model [9], in that deflection becomes more likely as interface cohesive strength decreases, interface toughness decreases, and relative material fracture length scale increases. One can also consider these trends in terms of material toughness, material strength, and the crack-tip stress field. As material toughness increases, the corresponding material strength requirement must be satisfied over an increasing distance. If the crack-tip field is incapable of providing the required stress over this distance, deflection occurs. This phenomenon causes the curvature observed in the figure. Varying incident angle shows, as expected, that deflection becomes more likely with decreasing incident angle with the greatest sensitivity (i.e. largest change in penetration / deflection behavior for a unit change in incident angle) at large angles. Also noteworthy is that an LEFM approach to the deflection-versus-propagation problem gives the same sensitivity trend (i.e. greatest sensitivity at large angles). Perhaps not expected is that as the incident angle is decreased, transition becomes increasingly strength-ratio dependent (i.e. the solid lines become increasingly vertical) with it being completely dependent on strength ratio, and independent of toughness ratio, at zero degrees.

The cause of this increasing dependence on strength ratio can be understood through an examination of the zero-degree case. Referring again to Figure 2-2, the zero-degree case is a degenerate case in which the angle ϕ has a value of zero and the interface becomes coincident with the x-axis. In this case, the interface is no longer diametral. It is radial. The radial portion of the interface corresponding to $x < 0$ and thus coincident with the crack is discarded, only the portion of the interface corresponding to $x > 0$ is retained. Thus the model geometry remains as a radial crack extending from the disk circumference to the disk center however the paths for propagation by penetration and propagation by deflection are now coincident and are aligned with the radial crack. As illustrated in Figure 2-5a for the first three cohesive-zone elements, the finite element mesh models this case by having the series of cohesive-zone elements for propagation by penetration (i.e. those extending into the material) parallel and adjacent to the series of cohesive-zone elements for propagation by deflection (i.e. those along the interface).

In the zero-degree case, both series of elements are aligned for pure mode I crack propagation in the same direction in the same crack-tip stress field. Identical loading (stress) is applied to each series of elements. Under these conditions the weaker (lesser cohesive strength) series of elements controls the development of the process zone, as shown in Figure 2-5b for three cohesive zone elements. The magnitude of stress in the process zone can never rise above the lesser cohesive strength due to fracture of the weaker cohesive zone elements. Thus fracture always occurs in the series of weaker elements regardless of toughness. In other words, displacement will preferentially occur in the weaker elements, precluding fracture of the stronger elements resulting in a completely strength-dependent criterion for the crack propagation path.

These arguments, valid for the zero-degree degenerate case, are also applicable to small angles but decreasingly as the incident angle increases. For incident angles near but not equal-to zero degrees, the two series of elements are nearly parallel and adjacent, are subjected to nearly the same stress field, and propagate in nearly the same direction. Correspondingly, for these small angles, transition between penetration and deflection is nearly completely strength-ratio dependent (i.e. the transition curve is nearly vertical). As the incident angle becomes greater, the orientation and loading of the elements increasingly differs, and both the strength ratio and the toughness ratio are relevant in determining if propagation occurs by penetration or deflection (i.e. the transition curve is neither vertical nor horizontal)

It is important to distinguish between criteria for propagation path determination (penetration or deflection) and propagation behavior after a path has been determined. As described, propagation path determination is a function of strength-ratio alone (true for zero-degree degenerate case and nearly true for small angles) or strength ratio and toughness ratio (true for larger angles). However, propagation behavior after a path has been determined, assuming fracture length scales are small, tends to LEFM predictions and is toughness controlled.

The effect of small, but varying, fracture length scale was studied by varying the parameter $\bar{E}\,\Gamma_i/\hat{\sigma}_i^2 R$. Material-to-interface strength ratio and toughness ratio at the transition between penetration and deflection were calculated for $\bar{E}\,\Gamma_i/\hat{\sigma}_i^2 R$ varying from 0.1 to 0.001; angles of 0°, 45°, 75° and 90°; and $\Gamma_m/\bar{E}R$ equal to 10^{-6}. The results are illustrated in Figure 2-6 where formatting and labeling are consistent with the prior figure. These results show that transition strength and toughness ratios decrease with decreasing interface fracture length scale (i.e. the curves move to the left and deflection becomes more likely) all else equal. However, decreasing

material fracture length scale, all else equal, enlarges the region corresponding to penetration. This trend is consistent with prior work for normally incident angles [21]. All fracture length scales converge to a strength-only criterion (i.e. a vertical line) for the zero-degree case.

The effect of variation of the parameter $\Gamma_m/\bar{E}R$ was considered under conditions of small and equal fracture-length scales. Physically, the value of $\Gamma_m/\bar{E}R$ can vary widely. For example, the dimension R can correspond to the size of a macroscopic object or a material's grain size. In prior work, it has been stated that changes in the magnitude of this parameter did not have a significant effect on predictions of penetration versus defection [21]. The results shown in Figure 2-7 provide evidence to support this claim. The interface and material fracture length scales were set equal at values of 0.1, 0.01, and 0.001 and $\Gamma_m/\bar{E}R$ was varied from a value of 10^{-10} to 10^{-4} (note since the two fracture length scales are equal, the strength ratio can be included on a second vertical axis having a value equal to the square root of the toughness ratio). The circular markers indicate calculated data points. From these results, several important features are evident. First, and perhaps most significant, is that the transition strength and toughness ratios show little variation with changes in the value of $\Gamma_m/\bar{E}R$. For $\Gamma_m/\bar{E}R$ values less than 10^{-7}, the data curves are nearly horizontal and coincident and at values greater than 10-7 the deviation is small. Additionally, as also shown in previous figures, the sensitivity of transition strength and toughness ratios to changes in the magnitude of the incident angle decreases as incident angle decreases (e.g. the distance between the 90° curves and the 75° curves is greater than that between the 45° and 0° curves). Also significant is that because the fracture length scales are small, the LEFM solution is recovered at an incident angle of zero degrees which corresponds to a single crack tip under mode I loading. Additionally, since fracture-length scales are small, the LEFM solution is recovered at an incident angle of zero degrees.

2.4. Conclusion

In this paper a combined stress-and-energy approach was used to explore the effect of incident angle magnitude on crack propagation direction for a crack incident to an interface. A cohesive-zone approach was implemented in a circular model subjected to LEFM mode I displacements. It was shown that when the crack-tip process zone was small, applying the mode I displacement boundary condition results in a K-field at the crack tip. When the process zone is not small a crack-tip K-field does not exist. As expected, small incident angles, relatively low strength interfaces, and relatively low toughness interfaces promoted deflection. However not expected was the finding that the transition between deflection and penetration becomes increasingly dependent on the ratio between material-and-interface strength as incident angle decreases becoming completely strength-ratio dependent (i.e. no dependence on toughness) at an incident angle approaching zero degrees. An examination of the zero-degree a case, using an arbitrarily shaped traction law, shows this behavior is a consequence of the penetrating and deflecting crack-tip process zones existing in a common stress field. Also it was shown that the sensitivity of transition conditions (i.e. material-and-interface strength and toughness ratios) to incident angle was greatest at large angles, becoming quite insensitive at angles approaching zero degrees. Finally, changes in the magnitude of the normalized-toughness dimensionless group, $\Gamma_m/\bar{E}R$, was shown to have little effect on transition conditions for equal and small material and interface fracture length scales with the LEFM solution being recovered at zero degrees.

These results are perhaps most significant in the simplification they present. While it has been shown that a stress-and-energy approach is needed for a general solution of the penetration-

deflection problem, implementation of this solution is not trivial with a number of parameters to be considered. Understandably this can lead researchers to continue to use other methods not because they are more accurate but because they are tractable. The results given in this paper identify regions where some parameters have little or no effect. This greatly simplifies the use of a stress-and-energy approach and, hopefully, will encourage its use for more accurate predictions of propagation behavior.

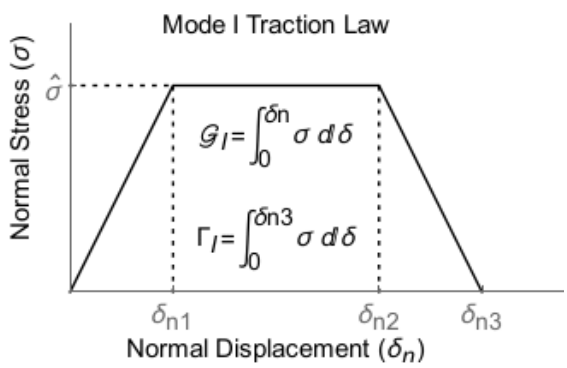
Mode I Traction Law
Normal Stress (σ)
$\hat{\sigma}$
$\mathcal{G}_I = \int_0^{\delta n} \sigma \, d\delta$
$\Gamma_I = \int_0^{\delta n3} \sigma \, d\delta$
δ_{n1}
δ_{n2}
δ_{n3}
Normal Displacement (δ_n)

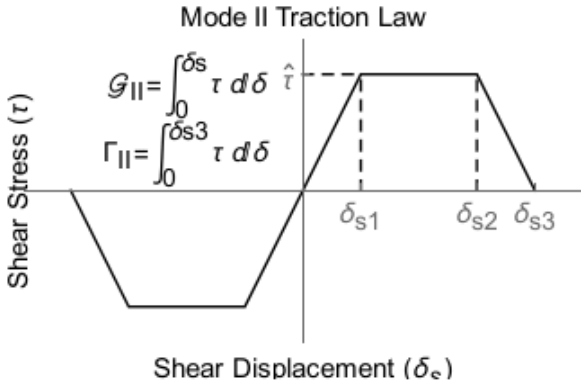
Mode II Traction Law
Shear Stress (τ)
$\mathcal{G}_{II} = \int_0^{\delta s} \tau \, d\delta$
$\hat{\tau}$
$\Gamma_{II} = \int_0^{\delta s3} \tau \, d\delta$
δ_{s1}
δ_{s2}
δ_{s3}
Shear Displacement (δ_s)

Figure 2-1: Traction laws showing crack-tip stress as a function of displacement for (a) mode I and (b) mode II loading.

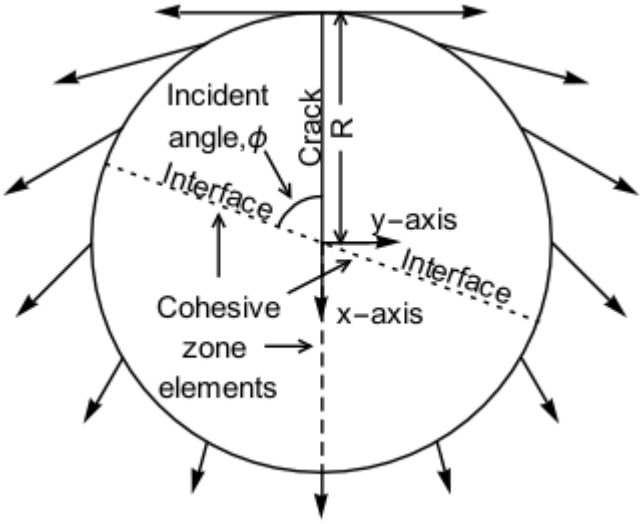

Figure 2-2: Finite element model geometry showing coordinate axes, displacement boundary conditions, radial crack, interface oriented at incident angle ϕ, and cohesive zone placement.

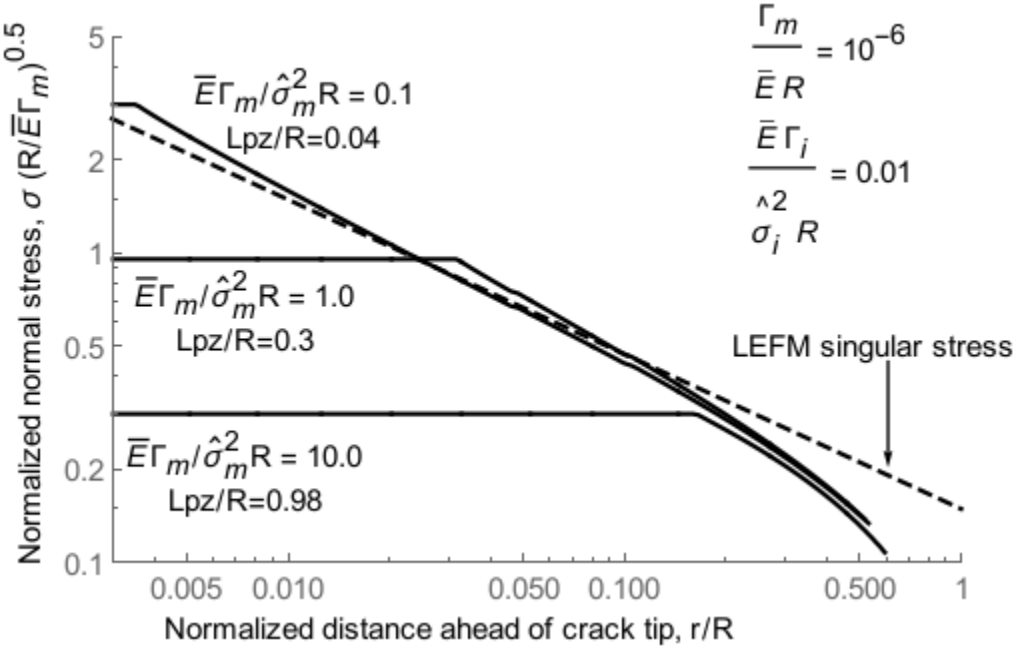

Figure 2-3: Normalized crack-tip opening stress as a function of normalized opening displacement showing the existence of an LEFM stress field at small values of material fracture length scale and process zone length.

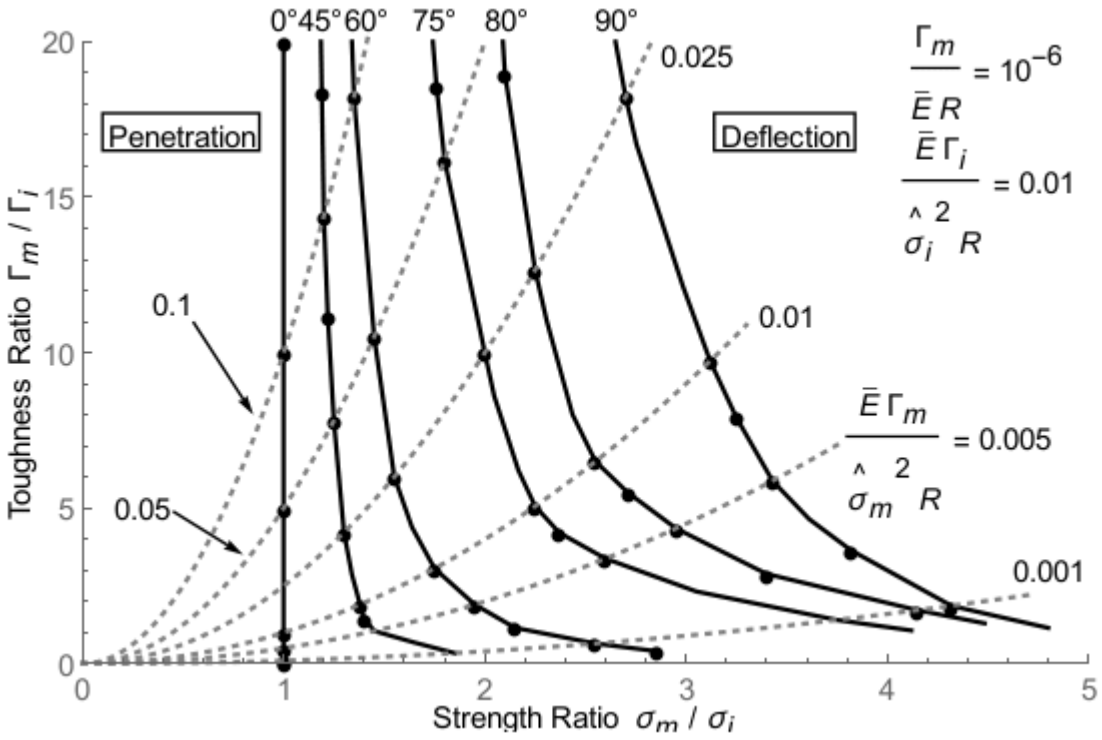

Figure 2-4: Material-to-interface strength and toughness ratios corresponding to transition between deflection and penetration (solid lines) for incident angles from 0° to 90° at a fixed interface fracture length scale and fixed normalized toughness and a range of material fracture length scales (dashed lines)

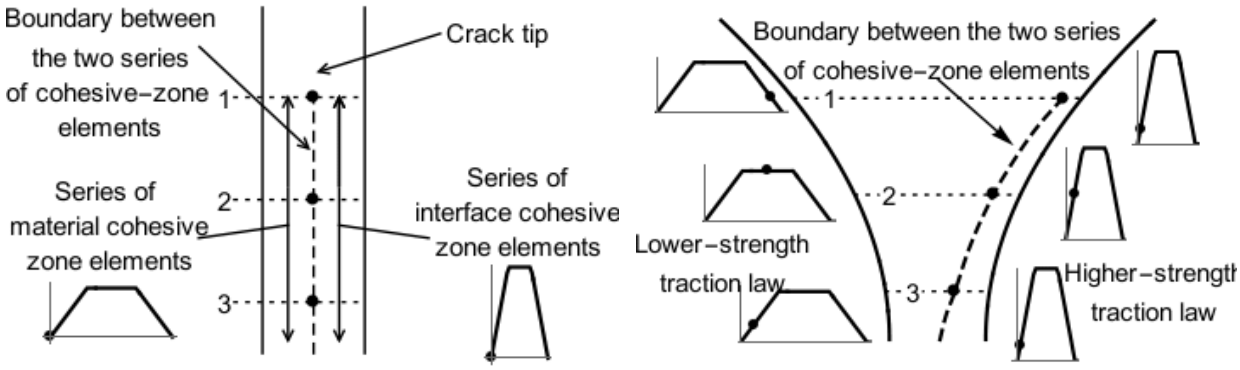

Figure 2-5: Three material and three interface crack-tip cohesive zone elements in the zero-degree degenerate case under (a) no load and (b) loading approaching fracture of element three

showing that elements corresponding to the lower-strength traction law control when fracture occurs.

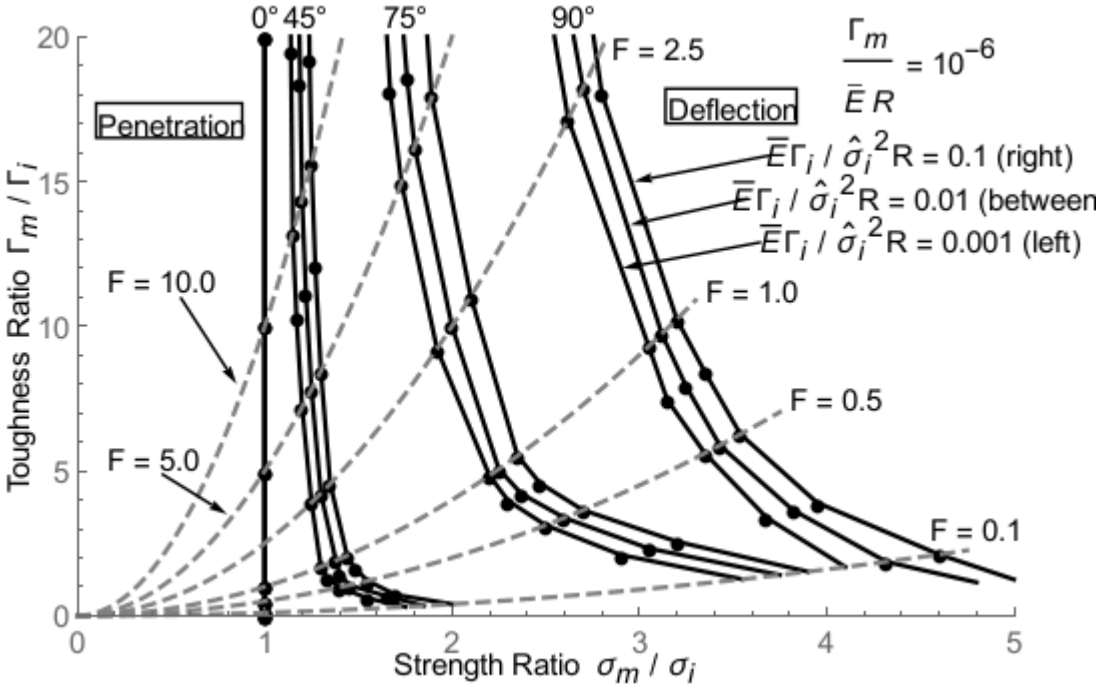

Figure 2-6: Data of Figure 2-4 for 0°, 45°, 75°, and 90° extended to show, right to left for each, the effect of varying interface fracture length scale, $\bar{E}\ \Gamma_i/\hat{\sigma}_i^2 R$ = 0.1, 0.01, and 0.001 where the parameter F gives the value of the material fracture length scale as $\bar{E}\ \Gamma_m/\hat{\sigma}_m^2 R$ = F ($\bar{E}\ \Gamma_i/\hat{\sigma}_i^2 R$).

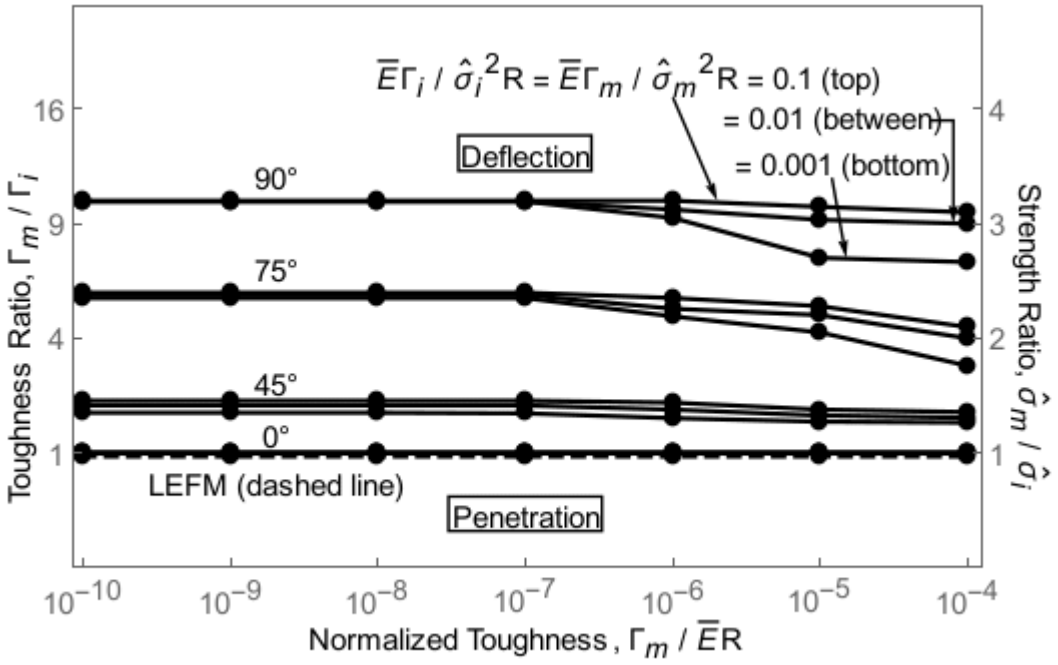

Figure 2-7: Effect of normalized toughness on transition strength and toughness ratios at equal and small fracture length scales over a range of incident angles.

Chapter 3 : Crack-Tip Interface Phase Angle for Mode-I Remote Loading

3.1 Introduction

Crack propagation behavior among constituent materials influences macroscopic material fracture properties of composites and laminates. For example, if an incident crack deflects along a constituent interface its overall propagation is inhibited which tends to increase macroscopic material toughness. If instead it penetrates across the interface this inhibition does not occur, decreasing toughness.

The significance of deflection versus penetration behavior is reflected in the large number of publications on this topic. The earliest work considered only the strengths of the interface and base material and defined critical strength ratios which predicted the transition between propagation by deflection and propagation by penetration [16, 28]. Later, linear elastic fracture mechanics (LEFM) was used resulting in critical toughness ratios being defined to predict deflection versus penetration behavior [17, 19]. More recently, criteria using both strength and toughness ratios have been used [14, 21]. Most recently, work has been done to unify these three approaches and show that strength-ratio is the controlling parameter under some conditions, toughness-ratio under others, and both are special cases of the general strength-and-toughness approach. Specifically, the relative strengths of the interface and base material alone tend to determine if deflection or penetration occurs when the angle between the incident crack and the interface is small (i.e. the incident crack approaches alignment with the interface) [24]. This is due to the deflecting and penetrating propagation paths sharing common stress and displacement fields. Conversely, the relative-toughness alone becomes the controlling parameter under

conditions distant from those corresponding to the transition between propagation by deflection and propagation by penetration. This is due to the LEFM approach using two discrete geometries, one for propagation by deflection and a second for propagation by penetration. Under conditions distant from those corresponding to transition there is little interaction between deflection and penetration. Propagation is distinctly one or the other and two discrete geometries model the problem well resulting in relative toughness being an accurate predictor of propagation behavior. At or near conditions corresponding to transition significant interaction occurs between the incipient propagation by deflection and the incipient propagation by penetration which the LEFM approach is unable to capture [23]. The combined strength-and-toughness approach captures interactions to whatever extent they occur and offers a general solution to the deflection versus penetration problem.

In addition to relative strength and toughness, understanding the fracture modes driving crack propagation is important. In a homogeneous isotropic material, crack propagation occurs by mode I (opening mode) alone. However, if the propagation is constrained to a particular path, other modes can contribute. An example, which is relevant to the work discussed in this paper, is two-dimensional propagation along an interface where both mode I and mode II (shear mode) can drive crack propagation. The relative contributions of mode I and mode II is typically quantified by a phase angle. Pure mode I corresponds to a phase angle of 0°, pure mode II to an angle of 90°, and angles between 0° and 90° to a combination of mode I and II (i.e. mixed-mode). A consideration of mixed-mode loading is critical in predicting deflection versus penetration behavior. For example, strength-based approaches typically assume only mode I drives both propagation by penetration and by deflection which greatly affects the resulting deflection-versus-

penetration predictions [21]. Despite this importance, a focused investigation of phase angle for the defection/penetration problem has not previously been published.

This paper uses a strength-and-energy approach to consider the phase angle of the propagating crack for the deflection/penetration problem. The analysis is conducted using a cohesive-zone approach which is implemented as a user-defined element in a commercial finite element package. Important aspects of the study include: the use of dimensionless groups in order to generalize results, comparison to existing LEFM solutions where possible, presentation of results both near and distant from transition conditions, and consideration of modulus mismatch (i.e. non-zero values of Dundur's alpha parameter). The remainder of this paper is organized as follows: the cohesive zone, finite element model, and dimensionless groups used are described, results are then presented, and finally conclusions are given.

3.2 Methods

3.2.1 Cohesive-zone model

The cohesive zone approach used in this study follows the work of Thouless [21, 22, 36, 39]. It includes two trapezoidal-shaped traction-separation laws which give the relationship between stress and displacement in the process zone ahead of the crack tip. One of these traction laws describes mode I fracture as shown in Figure 3-1a. The mode I strength, $\hat{\sigma}$, is given by the maximum stress reached on the traction-law curve. The mode I toughness, Γ_I, and mode I energy release rate, G_I, are given by the total and instantaneous areas under the traction-law curve respectively. The displacements δ_{n1}, δ_{n2}, and δ_{n3} define the shape of the mode I trapezoid. The other traction law, shown in Figure 3-1 b, describes mode II fracture and gives the corresponding mode II strength, $\hat{\tau}$, toughness, Γ_{II}, and energy release rate, G_{II}. The displacements δ_{t1}, δ_{t2}, and

δ_{t3} define the shape of the mode II trapezoid. For mixed-mode fracture, the normal and shear traction laws are combined by a linear fracture criterion given by

$$\frac{G_I}{\Gamma_I} + \frac{G_{II}}{\Gamma_{II}} = 1 \tag{3.1}$$

The relative amounts of mode I and mode II loading are quantified by the phase angle defined as

$$\psi = \tan^{-1}(\sqrt{G_{II}/G_I}) \tag{3.2}$$

Figure 3-2 illustrates the relationship between the two toughnesses, the two energy release rates, and the phase angle for the case of equal mode I and mode II toughnesses (i.e. $\Gamma_I = \Gamma_{II}$). This figure shows that for pure mode I fracture, $G_I/\Gamma_I = 1$, the phase angle equals zero degrees; for pure mode II fracture, $G_{II}/\Gamma_{II} = 1$, the phase angle equals ninety degrees; and for mixed-mode fracture, as governed by Eqn. 3.1, the phase angle is between zero and ninety degrees.

3.2.2 Finite Element Model

The commercial package Abaqus (version 6.13) was used for the finite element analysis. The cohesive-zone model was implemented through Fortran coding of the traction laws and fracture criterion in a user-defined element (UEL) subroutine in Abaqus similar to prior work [39]. The model geometry, shown in Figure 3-3, consisted of a circular disk with the interface along the horizontal diameter (y-axis) and the initial crack extending normally and radially upward (negative x-axis). Cohesive zone elements were placed where propagation was possible, i.e. along the interface and ahead of initial crack (i.e. along the positive x-axis, the positive y-axis, and the negative y-axis). Abaqus 2-D plane strain elements (CPE4R) were used elsewhere. A mesh convergence study was conducted to determine proper element size. The total number of elements were 48,390. Element size varied from smallest size 9e-4 mm x 9e-4 mm at the crack

tip to largest size 4.28 mm x 1.85 mm at the periphery of a 100 mm radius circular model. Boundary conditions consisted of displacements applied to the circumference of the model. Displacement values were calculated using the plane strain LEFM expressions for mode I loading of the initial crack as given by

$$u_x = \frac{K_I(1+v)}{E}\sqrt{\frac{R}{2\pi}}cos\left(\frac{\theta}{2}\right)\left[2-4v\ +2\,sin^2\left(\frac{\theta}{2}\right)\right] \tag{3.3}$$

$$u_y = \frac{K_I(1+v)}{E}\sqrt{\frac{R}{2\pi}}sin\left(\frac{\theta}{2}\right)\left[4-4v+2\,cos^2\left(\frac{\theta}{2}\right)\right] \tag{3.4}$$

Where the origin is at the center of the disk, u_x and u_y are the x-direction and y-direction displacements respectively, K_I is the mode I stress intensity factor, v is Poisson's ratio, E is Young's modulus, R is the radial distance from the origin, and θ is the counterclockwise-positive angular position with respect to the positive x-axes.

3.2.3 Material Properties and Model Parameters

The material properties and geometric parameters of the problem are as follows:

$$\delta_{1n}, \delta_{2n}, \delta_{3n}, \delta_{1t}, \delta_{2t}, \delta_{3t}, \Gamma_m\ , \Gamma_{Ii}\ , \Gamma_{IIi}, \hat{\sigma}_m\ , \hat{\sigma}_i, \hat{\tau}_i, \nu_1, \nu_2\ , \bar{E}_1, \bar{E}_2\ , R, \alpha, \beta$$

Where the δ traction-law parameters are as previously defined, Γ_m is the mode I toughness of material of the disk, Γ_{Ii} and Γ_{IIi} are the mode I and mode II toughnesses of the interface respectively, $\hat{\sigma}_m$ is the mode-I strength of the material of the disk, $\hat{\sigma}_i$ and $\hat{\tau}_i$, are the normal and shear interface strengths respectively, ν_1, ν_2 are the Poisson;s ratios of the material of the disk above and below the interface respectively, $\bar{E}_1 = E_1/1-\nu_1^2$ and $\bar{E}_2 = E_2/1-\nu_2^2$, E_1 and E_2 are the Young's moduli of the material of the disk above and below the interface respectively, R is

the radius of the circular disk as defined previously, and α and β are Dundur's parameters given by

$$\alpha = \frac{E_1 - E_2}{E_1 + E_2}$$
$$\beta = \frac{E_1(1-2v_2)/(1-v_2) - E_2(1-2v_1)/(1-v_1)}{2(E_1+E_2)} \quad (3.5)$$

These parameters can be translated to the following dimensionless groups using the Buckingham Pi theorem.

$$\frac{\delta_{n1}}{\delta_{n3}}, \frac{\delta_{n2}}{\delta_{n3}}, \frac{\delta_{t1}}{\delta_{t3}}, \frac{\delta_{t2}}{\delta_{t3}}\ \frac{\hat{\sigma}_i}{\hat{\tau}_i}, \frac{\Gamma_{IIi}}{\Gamma_{Ii}}, \frac{\hat{\sigma}_m}{\hat{\sigma}_i}, \frac{\Gamma_m}{\Gamma_i}, \frac{\Gamma_m}{\bar{E}_1 R}, \frac{\bar{E}_1 \Gamma_m}{\hat{\sigma}_m^2 R}, \frac{\bar{E}_1 \Gamma_i}{\hat{\sigma}_i^2 R}, \alpha, \beta$$

Where the traction-law shape parameters δ_{n1}/δ_{n3}, δ_{n2}/δ_{n3}, δ_{s1}/δ_{s3}, and δ_{s2}/δ_{s3} were held constant at values of 0.08, 0.90, 0.08, and 0.90 respectively, $\hat{\sigma}_i/\hat{\tau}_i$ and Γ_{Ii}/Γ_{IIi} were held constant at a value of one, and $\Gamma_i = \Gamma_{Ii} = \Gamma_{IIi}$. The group $\frac{\bar{E}_1 \Gamma_i}{\hat{\sigma}_i^2 R}$, is referred to as the *fracture length scale*. Its magnitude scales with the size of the process zone ahead of the crack tip [24]. A small fracture length scale is a necessary condition for agreement with LEFM results. The group $\frac{\Gamma_m}{\bar{E}_1 R}$, referred to as the *normalized toughness*, can span a wide range of magnitudes particularly if the parameter R is taken to be grain size (appropriate if granular fracture behavior is considered). An additional dimensionless group is used to quantify the load being applied to the circumference of the circular model. This is the loading causing the specified mode-I displacement boundary conditions. It is referred to as the *applied load* and is defined as $\sigma_0\sqrt{R/E\ \Gamma_i}$ where σ_0 is remote tensile stress calculated from peripheral reaction forces and associated areas.

3.3 Results

Results are first considered for conditions corresponding to the transition between propagation by penetration and propagation by deflection as a function of material-to-interface strength and toughness ratios. At this transition, significant process zones develop both along the interface (corresponding to incipient propagation by deflection) and across the interface into the base material (corresponding to incipient propagation by penetration). Data for no modulus mismatch ($\alpha = \beta = 0$) and $\Gamma_m/E\,R = 10^{-6}$ (a typical value for this parameter) is shown in Figure 3-4. Here the solid lines represent constant values for the interface fracture length scale, $\bar{E}\Gamma_i/\hat{\sigma}_i^2 R$, of 0.0005, 0.001, 0.01, and 0.1 as labeled in the figure. Each of these solid line indicates where transition occurs with penetration occurring to left of each and deflection occurring to right of each. The dashed lines indicate the value for the material fracture length scale, $\bar{E}\Gamma_m/\hat{\sigma}_m^2 R$, as a multiple of the interface fracture length scale. For example, the top most dashed line corresponds to $\bar{E}\Gamma_m/\hat{\sigma}_m^2 R = 2.5\,\bar{E}\Gamma_i/\hat{\sigma}_i^2 R$. These results, generated using a circular model, are consistent with prior work which used a rectangular model [21]. The fundamentally new data in this figure are the phase angle magnitudes for deflection (note that given the crack geometry and boundary conditions, as shown in Figure 3-3, propagation by penetration will always be pure mode I and thus have a phase angle equal to zero degrees). These angles are given for each point of intersection between the solid interface-fracture-length-scale lines and dashed material-fracture-length-scale lines. Along each material-fracture-length-scale line, these intersection points are numbered left-to-right one through four. These numerals correspond, left-to-right, to the four angles listed along the same material-fracture-length-scale line. For example, the deflection phase angles for equal material and interface fracture-length scales of 0.1, 0.01, 0.001, and 0.0005 are 12°, 15.5°, 22°, and 25.5° respectively. Overall, two trends are

evident. First, traversing a solid line top-to-bottom shows that for a constant interface fracture-length scale, phase angle increases with decreasing material fracture-length scale. Second, traversing a dashed line left-to-right shows that for both interface fracture-length scale and material fracture-length scale increasing in size simultaneously, phase angle decreases. Considered together, these two trends indicate that phase angle magnitude scales inversely with fracture length scale at transition. That is, when transition conditions correspond to relatively large fracture length scales, phase angle is relatively small and when transition conditions correspond to relatively small fracture length scales, phase angle is large. One can also think of this in terms of process-zone size. Relatively large process-zones at transition correspond to relatively small deflection phase angles and small process-zones to large deflection phase angles. Also of interest is the large variation in magnitude of the deflection phase angle from, perhaps surprisingly, nearly pure mode I (8.4°) to nearly 45°. This indicates the considerable significance of the effect of the interaction between the incipient propagation by penetration and the incipient propagation by deflection.

Transition conditions are next considered as a function of fracture length scale. It has been shown previously, using a rectangular model [23], that when the values of the interface fracture length scale, $\bar{E}\Gamma_i/\hat{\sigma}_i^2 R$, and the material fracture length scale, $\bar{E}\Gamma_m/\hat{\sigma}_m^2 R$, are simultaneously small that the applied load required for propagation at transition converges to an LEFM solution for short branching cracks emanating at 90° from the tip of a main crack under mode I loading [40]. Similar results, calculated for the circular model of this paper, are shown in Figure 3-5. In this figure, applied load (given as $\sigma_0\sqrt{R/E\ \Gamma_i}$) is shown on the right vertical axis as a function of equal interface and material fracture length scales. Convergence to the LEFM solution occurs as

fracture-length-scale magnitudes decrease. Also included in this figure (and not present in prior work) is a comparison of phase angle values. From the LEFM solution, the phase angle of the branching cracks emanating at 90° from the tip of the main crack is 24.85° [40]. This value is shown as a horizontal dashed line as read on the left vertical axis. The cohesive zone solution for phase angle of the deflecting crack is shown as a solid curve and converges to the LEFM value as fracture-length-scale value deceases.

Results are next considered for conditions corresponding to transition as a function of the normalized toughness, $\Gamma_m/E\ R$. Data is shown in Figure 3-6 for equal fracture length scales of 0.1, 0.01, and 0.001, and for normalized toughness values of 10^{-10} to 10^{-5}. The magnitude of the phase angle during transition decreases with decreasing normalized toughness and increasing fracture-length scale. The data trends suggest asymptotic values might exist at small normalized toughness values.

Consideration of conditions both near and far-from transition gives important insight into propagation behavior. As shown in prior work [14, 23] using a rectangular model, near transition and prior to propagation relatively large process zones develop both along the interface (corresponding to impending deflection) and in the base material (corresponding to impending penetration). When propagation occurs, one process zone evolves into a propagating crack and the other collapses. The creation of the two process zones creates an unstable energetically-elevated state which corresponds to a cusp in applied load. This cusp is illustrated, for the circular model of this paper, in the lower portion of Fig.6. Here the applied load is given by the dimensionless group $\sigma_0\sqrt{R/E\ \Gamma_i}$ (described previously) as a function of the ratio of material toughness to interface toughness for constant interface fracture length scale and varying material

fracture length scale. Transition corresponds to the maximum applied load and occurs at the tip of the cusp. Also shown in this figure is the phase angle of the propagating crack as a function of the same variables. A discontinuity in phase angle value occurs at transition. For a material-to-interface toughness ratio less than the transition value, propagation occurs by penetration and the phase angle of the propagating crack is zero degrees (i.e. pure mode I). For a material-to-interface toughness ratio greater than the transition value, propagation occurs by deflection and the phase angle of the propagating crack is non-zero (i.e. mixed mode) and varies in magnitude at transition with material fracture length scale. An examination of the magnitude of phase angle for propagation by deflection reveals two significant trends. First, the phase angle of the deflection crack has a minimum magnitude at transition, increasing as the material-to-interface toughness value increases beyond the transition value. Second, the deflection phase angle eventually appears to reach an asymptotic value at relatively large material-to-interface toughness values. When both interface and material fracture length scale values are small, this asymptotic value corresponds to the LEFM value of 38.9° for propagation of a crack along an interface [19, 39]

The effect of modulus mismatch on the deflection phase angle is considered next. Durdur's alpha parameter was varied from -0.7 to 0.7. As shown in Eqn. 3.5, positive values of alpha correspond to a stiffer material above the interface (i.e. along the negative x-axis in Figure 3-3) and more compliant material below the interface. Negative values of alpha correspond to the reverse. Dundur's beta parameter was held equal to zero. Applied load and phase angle results are shown in Figure 3-8 for small and equal fracture-length-scales of $\bar{E}\Gamma_i/\hat{\sigma}_i^2 R = \bar{E}\Gamma_m/\hat{\sigma}_m^2 R$=0.001, and a normalized toughness of $\Gamma_m/\bar{E}R$=10^{-6}. Consistent with prior work using a rectangular model [23], the applied load at transition for the circular model of this paper

reaches a maximum at the greatest magnitude of negative alpha and monotonically decreases to a minimum value at the greatest positive magnitude. Two curves are shown for phase angle of the deflecting crack. The first corresponds to conditions far from transition and thus the value for alpha equals zero is 38.9° as also shown in Figure 3-8. Along this curve, phase angle increases with increasing positive alpha magnitudes, apparently approaching an asymptotic value of approximately 72°. Similarly, phase angle decreases with increasing negative alpha magnitudes, apparently approaching an asymptotic value of approximately 9°. The second curve for deflecting phase angle corresponds to transition conditions. It follows the same trend as the first curve but having lesser phase angle magnitudes for each alpha value. The difference being greatest at alpha equals zero and decreasing, to nearly zero, at extreme positive and negative alpha values.

3.4 Conclusions

In this paper energy-and-strength based cohesive-zone model was utilized to investigate mixed-modeness of interface in terms of phase angle at crack-tip for mode-I remote loading. A reduced circular model was used for computational convenience and the deflection boundary conditions were derived for mode-I using LEFM. Results were presented in terms of dimensionless groups for a wide range of material systems. It was illustrated that the behavior determined by energy-based LEFM method and cohesive zone method agrees for a complete deflection. Penetration, transition and deflection were controlled varying material-to-interface toughness ratio and stress ratio. Results showed that crack-tip interface phase angle is lower while the corresponding applied load is higher at or near transition moving

from deflection. There is a discontinuity of zero-phase angle during penetration and non-zero-phase angle at transition. The interface phase angle and applied load results at deflection (far from transition) were compared and found great agreement with LEFM solution, provided the material and interface fracture-length-scales are small enough to meet LEFM criterion. The effect of the dimensionless group material-normalized-toughness, $\Gamma_m/\bar{E}R$, was investigated and concluded small effect on interface mixed-modeness at transition, especially when both interface and material fracture-length-scales are large. Finally, it explored the effect of elastic-mismatch varying Dundurs' alpha while beta was constant at zero. Results illustrated that interface-phase-angle is smaller for more compliant pre-cracked material, while interface-phase-angle is higher for stiffer pre-cracked material during transition and also at complete deflection. It also showed two possible asymptotes of interface-phase angle at low and high Dundur's α.

The results and conclusion in this paper is remarkable in the sense of understanding the interface mechanism during transition between penetration and deflection. It is proved that energy-and-stress method is not only widely capable of capturing the general cases of penetration, and deflection but also the transition between penetration and deflection.

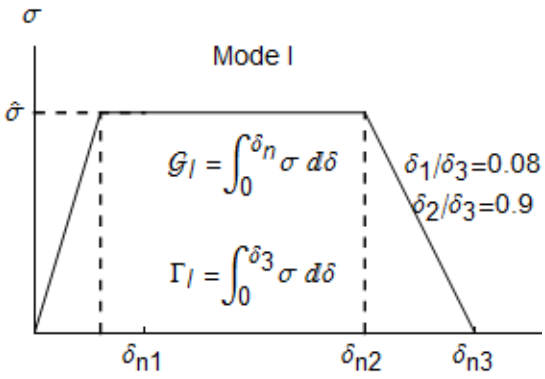
σ
Mode I
σ̂
$\mathcal{G}_I = \int_0^{\delta_n} \sigma \, d\delta$
$\Gamma_I = \int_0^{\delta_3} \sigma \, d\delta$
δ_1/δ_3=0.08
δ_2/δ_3=0.9
δ_{n1}
δ_{n2}
δ_{n3}

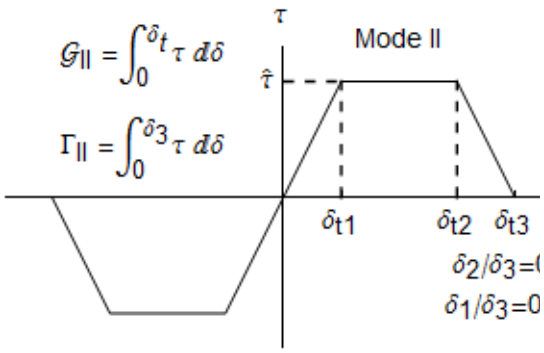
τ
Mode II
$\mathcal{G}_{II} = \int_0^{\delta_t} \tau \, d\delta$
$\Gamma_{II} = \int_0^{\delta_3} \tau \, d\delta$
τ̂
δ_{t1}
δ_{t2}
δ_{t3}
δ_2/δ_3=
δ_1/δ_3=0

Figure 3-1: Traction separation laws of the cohesive zone elements that shows maximum strength at the end of linear-elastic zone, no stress change for a certain deflection of plastic zone, and at last stress reduction (a) mode I and (b) mode II loading.

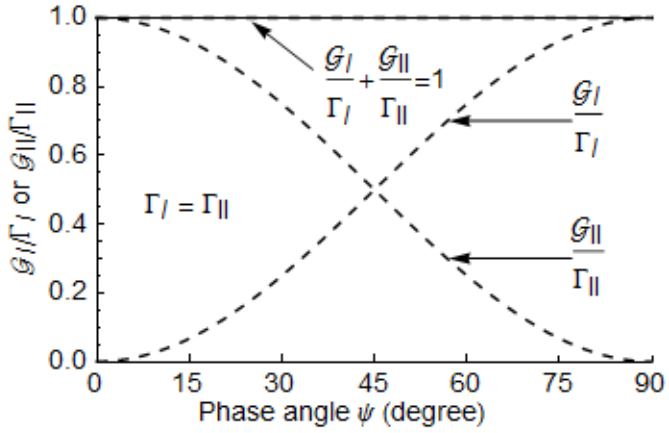

Figure 3-2: Dependence of the ratio of energy release rate and toughness on nominal phase angle.

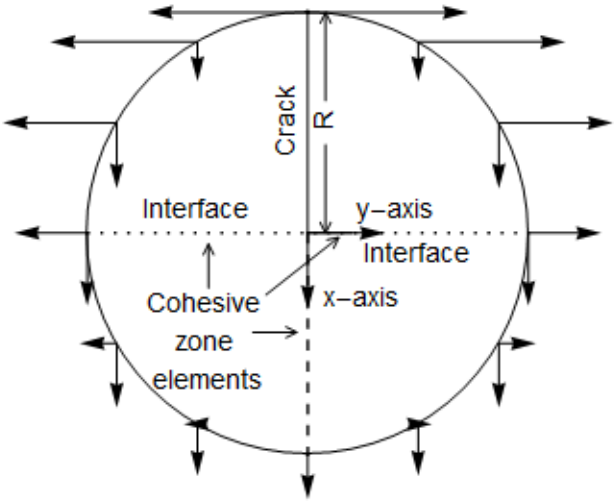

Figure 3-3: Circular model geometry that has been considered as finite element model in our study, illustrating displacement boundary conditions, coordinate axes, crack from center to perimeter of the disk, and cohesive zone elements in the radial directions.

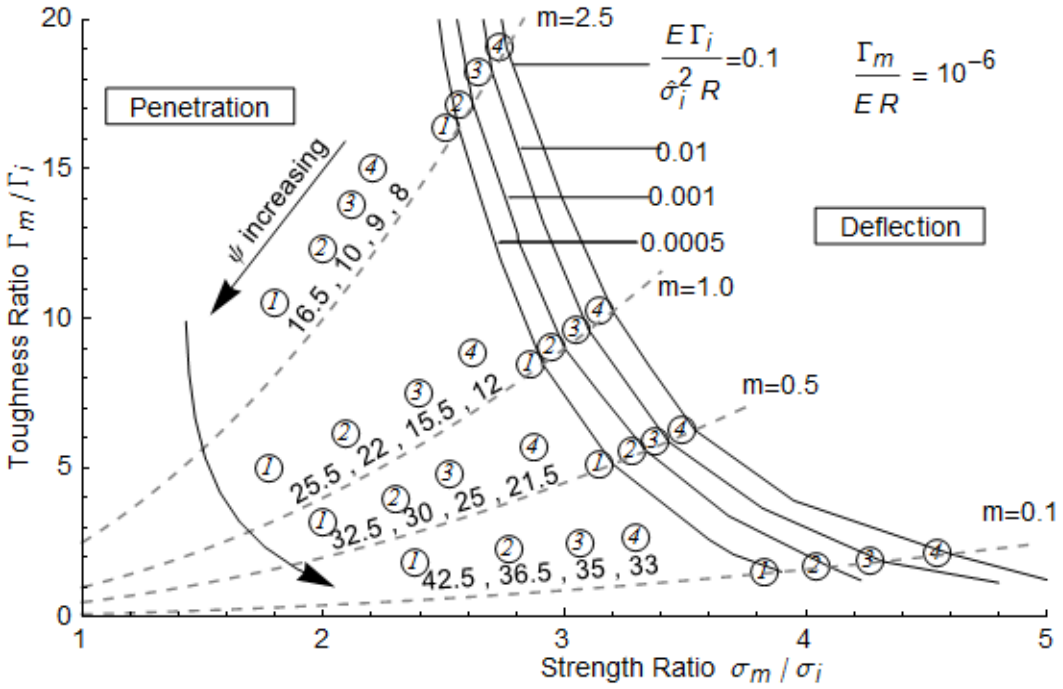

Figure 3-4: Material-to-interface strength and toughness ratios at transition between deflection and penetration (solid lines) varying interface and material-fracture-length-scales for constant Γ_m/ER = 10^{-6}, α = 0, β = 0. The numbers along the dashed lines are phase angles, ψ, for constant material-fracture-length-scale that constitute indices for finding their corresponding points for

$\bar{E}\Gamma_i/\hat{\sigma}_i^2 R$=0.1, 0.01, 0.001, and 0.0005 in the solid lines. The multiplier 'm' gives the material-fracture-length-scale as $\bar{E}\Gamma_m/\hat{\sigma}_m^2 R$ = m ($\bar{E}\Gamma_i/\hat{\sigma}_i^2 R$).

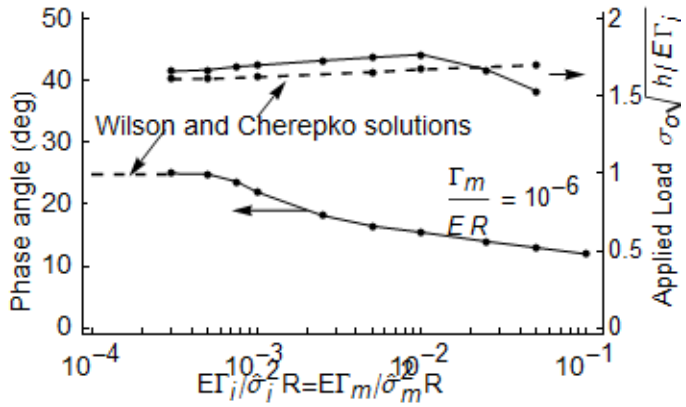

Figure 3-5: Phase angle and applied load at transition as a function of equal material and interface fracture-length-scale ($\bar{E}\Gamma_i/\hat{\sigma}_i^2 R=\bar{E}\Gamma_m/\hat{\sigma}_m^2 R=\bar{E}\Gamma/\hat{\sigma}^2 R$), and showing agreement with LEFM based results for three kink cases along penetration, left-deflection, and right-deflection.

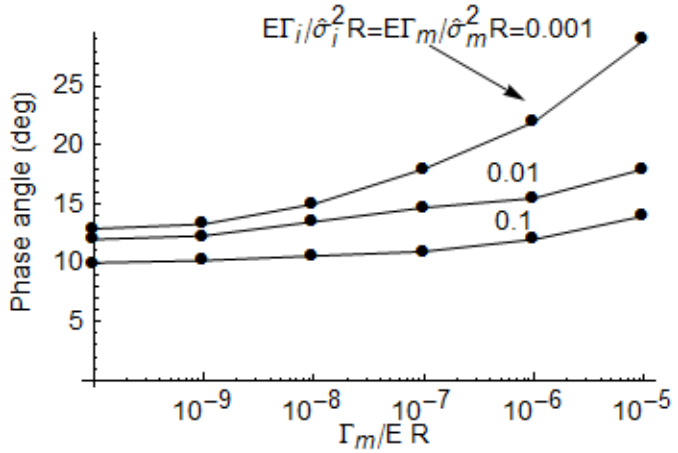

Figure 3-6: Effect of normalized toughness at crack-tip interface phase angles for a set of equal fracture-length-scales $\bar{E}\Gamma_i/\hat{\sigma}_i^2 R$ = $\bar{E}\Gamma_m/\hat{\sigma}_m^2 R$ =$\bar{E}\Gamma/\hat{\sigma}^2 R$ = 0.001, 0.01, and 0.1. Solid lines

indicate the interface-phase-angle trend line during transition for a constant equal fracture-length-scale.

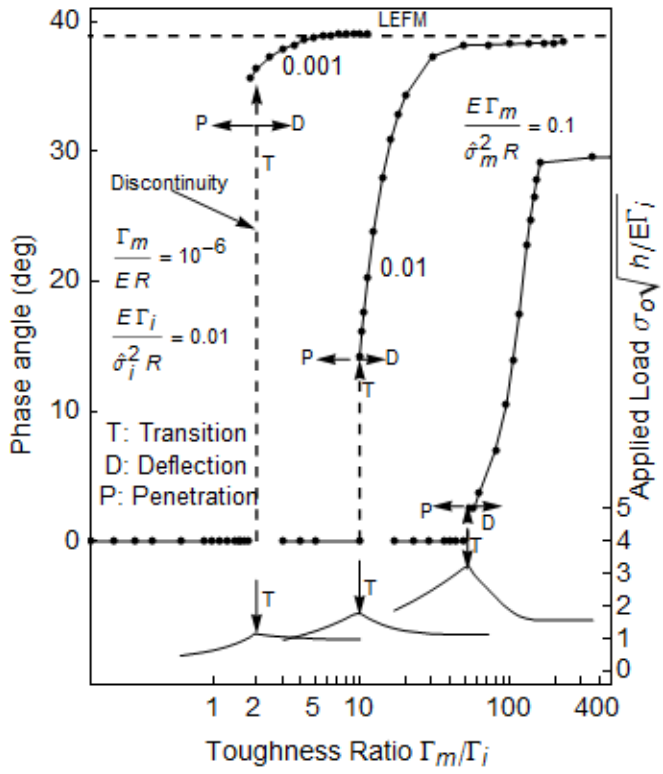

Figure 3-7: Phase angle and required applied load during transition as a function of material-to-interface toughness ratio. The dashed arrow showed the discontinuity of phase angle at transition between penetration (zero-degree phase angle points situating left of dashed lines) and deflection

(right of the dashed lines). The effect of varying material fracture-length-scale at 0.001, 0.01, and 0.1, from left to right, showed for constant $\bar{E}\Gamma_m/\hat{\sigma}_m^2 R$= 0.01 and $\Gamma_m/\bar{E}R$ = 10^{-6}.

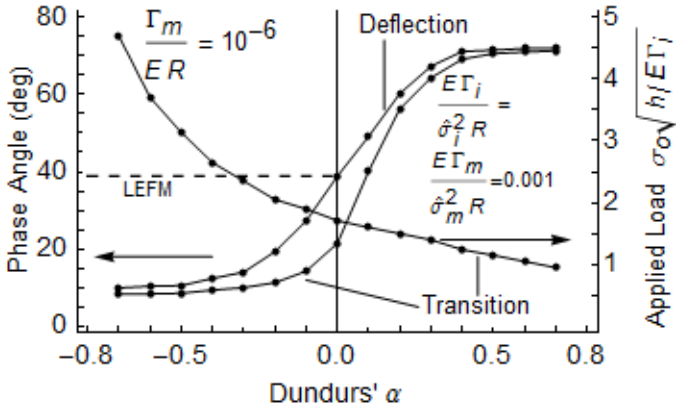

Figure 3-8: Applied load and phase angle at transition as a function of Dundurs' parameter α, for β=0, $\bar{E}\Gamma_i/\hat{\sigma}_i^2 R = \bar{E}\Gamma_m/\hat{\sigma}_m^2 R$=0.001, and $\frac{\Gamma_m}{\bar{E}R}$=$10^{-6}$. Interface phase angle at deflection far from transition also showed as a function of α.

Chapter 4 : An Experimental Assessment of Models to Predict Crack Deflection at an Interface

4.1 Introduction

One of the most important questions regarding the fracture behavior of composites and laminated materials is whether a crack will deflect along, or penetrate though, an interface. This is because interfaces play a major role in their mechanical properties. Considering the case of a fiber reinforced composite, there are numerous interfaces between the matrix and the fibers. When a crack propagates through the matrix and fibers without deflecting, the strength and toughness of the composite is not improved much compared to the matrix material since little additional energy dissipates through this kind of penetration cracking process. On the contrary, if a crack deflects around the fibers, this process involves the creation of more crack surface area and fiber bridging processes giving more energy dissipation and stronger, tougher composites. The same benefit of interfacial crack deflection occurs for toughened ceramics [5], laminated materials [21], polycrystalline materials [41, 42], and natural composites (e.g., wood, oyster shell, etc.) [10, 43].

In order to understand whether a crack will penetrate or deflect when propagating through a composite, one must model the behavior in terms of the interface and bulk material properties along with other geometric parameters. The earliest approach to predict crack penetration versus deflection was based on material strength [28]. They considered a crack incident to a fiber at an angle of 90° in a brittle material system where the elastic properties of the matrix and fiber are the same. Using the stress around crack tip that was derived from [44], they found that the stress in front of a crack tip parallel with crack plane is five times more than the stress perpendicular to

the crack plane. Based on this analysis they hypothesized that the fiber strength should be at least five times the strength of the interface to create transition from penetration to deflection. Extending this work [16] developed a crack penetration versus deflection criterion for a bi-material system. They used stress fields derived in earlier work [44, 45] also for a crack 90° incident to an interface. The ratio of maximum stress across the interface and along the interface were used to predict deflections for a wide range of bi-material systems including homogeneous system. It has been found from their analysis, for a homogeneous system, a crack should deflect if the cohesive strength across the interface is three and half times stronger than the adhesive strength of interface. Note that the magnitude of strength ratio from their analysis is smaller than the strength ratio provided from [28] for crack deflection. However, the strength ratio can be higher for stiffer first phase materials and the opposite is true for more compliant materials.

A more recent approach for determining crack penetration versus deflection criterion at interfaces, energy-based approach, that was developed by Rice [46]. He followed Griffith's energy based model [47] and modified Griffith model [48, 49]. Later many researchers applied linear elastic fracture mechanics (LEFM) for defining the conditions under which crack deflection along an interface would occur [30, 50, 51]. They calculated energy release rate for kinks, along the crack plane and perpendicular to the crack plane, starting from the crack tip following the work by Cotterell and Rice [52]; and considered the energy release rate has to be proportional to the toughness to propagate crack in a direction. The result published by He and Hutchinson [50] predicted that for an elastically homogeneous material system with a crack 90° incident to an interface, the crack deflects when second phase material toughness, given in terms of the critical strain energy release rate, is greater than four times the toughness of interface. This energy based approach result has been heavily cited in recent years.

Assessing the approaches described above, the strength based approach [16, 28, 45] does not consider the relative toughnesses and energy based method [30, 50, 51] does not consider the relative strengths of the materials and the interface. An alternative approach, the cohesive zone method [53, 54] , considers both strength and toughness in the fracture criterion and was first applied to the interface crack deflection problem by Parmigiani and Thouless [21]. They showed that the energy based method result is a special case solution of the cohesive zone method; the cases for small fracture-length scales that represent brittle materials. Furthermore, it has been argued that the cohesive zone model is applicable for a wider range of materials with no restriction of the presence of kinks, as it is in energy-based methods, and incident angles [21, 24, 55, 56]. However, to date there has not been an experimental validation of those results to determine which approach best predicts crack deflection versus penetration at real material interfaces.

Accordingly, this paper presents an experimental study to determine the crack penetration/deflection behavior at bonded polymethyl methacrylate (PMMA) interfaces and compare those results to predictions based on the different methods. Additionally, to illustrate the importance of considering both the toughness and strength ratios, two different commercially available solvents were chosen to create interface bonds with similar toughness but different adhesive strengths. The results of this experimental study provide insight into the drawbacks and benefits of different crack penetration/deflection prediction methods.

4.2 Models for Predicting Crack Deflection versus Penetration

Consider a crack incident on an interface at an angle ϕ in a linear elastic, elastically homogeneous material under mode-I remote applied stress. As shown in Figure 4-1, the crack may propagate across the interface towards second phase (penetration) or along the interface (deflection). The interface in Figure 4-1 is denoted by dotted line. The key question to be addressed is what is the correct criterion to accurately predict the direction of crack propagation, i.e., penetration or deflection. The next sections will examine two criteria based on: 1) the energy-based approach of He and Hutchinson [17] that relies on the relative toughnesses of the material and interface, and 2) the cohesive zone based approach that accounts for both the relative toughnesses and strengths.

4.2.1 Energy based criterion for deflection

Energy based methods by He and Hutchinson [17] established a criterion for crack penetration/deflection for static remote loading. They proposed that penetration occurs when crack energy release rate G_I^p reaches the mode-I fracture toughness of substrate Γ_I^s by a stress intensity factor K_I^p.

$$G_I^p = \frac{(K_I^p)^2}{E'} = \Gamma_I^s \tag{4.1}$$

Young's modulus, and Poisson's ratio are denoted by E, and ν respectively, and $E' = E / 1 - \nu^2$ for plane strain and $E' = E$ for plane stress. The energy release rate can be calculated from the magnitude of loading, elastic constants, and geometry while the fracture toughness is determined

from experiments. Conversely, the criterion for crack deflection at the interface requires both the shear stress intensity factor K_{II}^{i} and normal stress intensity factor K_{I}^{i} to calculate energy release rate.

$$G^{i} = \frac{\left(K_{I}^{i}\right)^{2} + \left(K_{II}^{i}\right)^{2}}{E'} = \Gamma^{i} \tag{4.2}$$

The two stress intensity factors at interface are a function of remote normal loading stress intensity factor and the interface angle, ϕ [51, 57, 58].

$$\begin{aligned} K_{I}^{i} &= K_{I}^{p}\left(\frac{3}{4}\cos\frac{\phi}{2} + \frac{1}{4}\cos\frac{3\phi}{2}\right) \\ K_{II}^{i} &= K_{I}^{p}\left(\frac{1}{4}\sin\frac{\phi}{2} + \frac{1}{4}\sin\frac{3\phi}{2}\right) \end{aligned} \tag{4.3}$$

From the above two equations the ratio of energy release rate as a function of interface angle is found.

$$\frac{G_{I}^{p}}{G^{i}} = \frac{1}{16}\left[\left(3\cos\frac{\phi}{2} + \cos\frac{3\phi}{2}\right)^{2} + \left(\sin\frac{\phi}{2} + \sin\frac{3\phi}{2}\right)^{2}\right] \tag{4.4}$$

Analyzing Eqn. 4.1 and Eqn. 4.2, fracture criteria can be set as follows:

$$\frac{G_{I}^{p}}{G^{i}} < \frac{\Gamma_{I}^{s}}{\Gamma^{i}} \tag{4.5}$$

for penetration, and

$$\frac{G_I^p}{G^i} \geq \frac{\Gamma_I^s}{\Gamma^i} \tag{4.6}$$

for deflection.

While the fracture toughness of a material may also be a function of the crack velocity [59], in the present study only quasi-static conditions are considered.

4.2.2 Cohesive zone model

Cohesive zone model (CZM) consists of traction laws, where stress is a function of displacement within the cohesive zone. The shape of the traction law can be of arbitrary shape, e.g., triangular, rectangular, or trapezoidal, and can be tailored to the properties of material. The CZM considered in the present study has two separate trapezoidal traction laws shown in Figure 4-2, one for normal stress and displacement (mode I) and another for shear stress and displacement (mode II). For the mode I traction law, the normal strength $\hat{\sigma}$ defines the peak stress in the cohesive zone and the material fails at the critical displacement δ_3. The traction law for shear stress and displacement is defined similarly and total area under that traction law is the toughness of the material. If the displacement is unable to reach the critical displacement δ_3, then the associated partial area of the trapezoid is the strain energy release rate of the material for those loading conditions.

While the normal traction law applies to pure mode-I loading and the shear traction law applies to pure mode-II loading, the mixed-mode case is given by a linear combination of the two traction laws:

$$\frac{G_I}{\Gamma_I} + \frac{G_{II}}{\Gamma_{II}} = 1$$

The effect of various model parameters on the crack deflection/penetration behavior has been computationally explored [21, 23, 24]. The energy-based and CZM model predictions agree under certain conditions of small fracture-length scales for penetration and deflection. The results also reveal a wide range of situations where the CZM predictions differ from the energy-based model. CZM considers cohesive zone in both of penetration and the deflection directions that is capable of capturing the competition during transition. On the contrary, energy-based LEFM uses predefined kink in penetration or deflection direction, which cannot show the competition during transition between penetration and deflection [23]. [24] showed a strong relation between crack penetration/deflection and incident angle.

4.3 Experimental Procedure

4.3.1 Materials

Polymethyl methacrylate, known as PMMA, was chosen as the model material for this study because it is a brittle material that exhibits predominantly linear elastic behavior. Furthermore, it is easy to form interfaces in PMMA using commercial solvents and PMMA has been utilized previously in the literature for experimental studies of interface fracture behavior [60, 61]. Since the mechanical properties of PMMA procured from different manufacturer can vary significantly [60], the PMMA used in this study was all bought from the same manufacturer (Evonik Cyro LLC, Parsippany, NJ, USA). Some physical and mechanical properties of the PMMA provided by the manufacturer are shown in Table 4-1.

To make interface samples, solvent adhesives were used that soften and bond the native PMMA without adding a layer of another polymer. This method was chosen to create a very thin (nearly zero-thickness) interface with minimal discontinuity in the elastic properties. Two types of interfaces were desired with similar mode I fracture toughness but different adhesive strengths. To achieve this, two different solvent based adhesives were used from the same manufacturer. Weld-On 4 (SCIGRIP, Durham, NC, USA) was chosen as a solvent adhesive giving medium strength joints while Weld-on 16 (SCIGRIP, Durham, NC, USA) was chosen to give higher strength. For all interface samples, the bonding surfaces were polished with 1200 grit sandpaper to make a smooth surface, cleaned using clean natural water and dry Kimwipes (Kimberly-Clark Professional, Roswell, GA, USA). Following the manufacturer instructions, all bonds were cured for 7 days at room temperature to get the full desired bonding strength.

4.3.2 Mechanical property measurements

Since accurate tensile strength and fracture toughness values of the PMMA were essential for accurate model predictions, values were measured in this study following ASTM standard D638-14 and D5045-99 for strength and toughness, respectively, rather than relying on the values quoted by the manufacturer. A constant sample thickness, B = 5.8 mm, was used for all specimens. The specimens were computer numeric control (CNC) machined to ensure the dimensional accuracy (VMC-4525, FadalCNC, Meridian, ID, USA). The tensile strength was measured using a computer-controlled electro-mechanical universal testing machine (5982, Instron Corporation, Norwood, MA, USA) using a displacement rate of 5.2 mm/min. The overall length and gauge length were 165 mm and 57.2 mm, respectively; all other dimensions are same as Figure 4-3 (a). The samples were held using mechanical wedge grips with serrated jaw faces. The number of replicates tested were five. The fracture toughness was measured using a

computer-controlled servo-hydraulic universal testing machine (8872, Instron Corporation, Norwood, MA, USA) with a capacitance based displacement transducer (HPT150, Capacitec Inc., Ayer, MA, USA) affixed to the clevises to measure the load-point displacement. A constant loading rate 10 mm/min has been used. At the end of the notch tip a sharp blade was tapped gently to create a sharp crack at the crack tip. Ten replicate tests were performed. Dimensions of the compact test specimen are same as Figure 4-3 (b). All the tests being placed at room temperature approximately 24° C.

There are no standards available for testing mechanical properties of adhesives for homogeneous or bi-material systems. Reference [62] discussed some methods for tensile strength testing and fracture toughness testing of adhesives in a homogeneous and bi-material system. Similar to the tensile test specimen used by [62], the tensile test specimen were fabricated in this study by joining two half-pieces of tensile specimen together under pressure using a custom fixture. The interface tensile sample dimensions (see Figure 4-3 (a)), and loading rate were chosen to be identical to those used above for measuring the PMMA tensile strength based on the ASTM standard D638-14 for strength testing of plastics. Similarly, non-standard test was designed for measuring the mode-I fracture toughness of the interfaces based on ASTM standard D5045-99 for plastics. The compact test specimens were fabricated by bonding two half-pieces together (see Figure 4-1(b)). A sharp razor blade was tapped gently into the notch to create a sharp crack at the interface. The dimensions (see Figure 4-3 (b)), loading rate and other properties were chosen similar to be identical to those used above for measuring the PMMA fracture toughness. Three replicate tests were performed for the fracture toughness of each adhesive.

4.3.3 Crack deflection sample design

In this experimental study, a single-edge-notch tensile test specimen was designed where the crack starts from a free edge and is incident on an interface (Figure 4-4). The interface orientation in the samples was varied to explore penetration-deflection behavior for various crack incident angles from ϕ = 75° - 90°. All the tensile test specimens were 305 mm long, 25.4 mm wide, and 5.8 mm thick. For all samples the initial crack was 2.54 mm long and was oriented perpendicular to the edge and incident on an interface at the middle of the specimen length (Figure 4-4). The initial crack length was chosen to be small compared to the in-plane samples dimensions while the specimen length was chosen to ensure uniform stress at the middle of the sample free from boundary effects. To assemble each sample, two pieces of PMMA were bonded to the third, biggest, piece above and below the precrack (Figure 4-4). The various incident angles, ϕ, were selected as 90°, 85°, 80°, and 75°. The specimens were CNC machined for dimensional accuracy similar to the specimens for strength and toughness measurements. Interfaces were made with two different strengths using the solvent based adhesives Weld-On 4 and Weld-On 16 by applying pressure using a custom fixture. The precrack was created using a piece of 0.03 mm thick Teflon tape in-between two pieces of PMMA in both sided of the crack.

4.3.4 Crack deflection mechanical testing

All the crack deflection specimens were tested in tension under displacement control using the same procedures described above for the measurement of tensile strength. For each combination of incident angle and solvent adhesive, 3-4 replicate tests were conducted. Samples were tested until the crack propagated through the whole width of each specimen. Crack penetration or deflection was determined by observing the crack propagation direction where the

precrack tip touches the interface (Figure 4-4). Penetration was considered when the crack propagated across the interface, while deflection was considered when the crack initially propagated along the interface. For the crack deflection cases, the crack would often subsequently kink into the PMMA after initiating deflection at the interface and return to a nominally mode I path. To observed even very small deflections, a digital camera (WG-4, Ricoh, Tokyo, Japan) was positioned nearly perpendicular to the plane of specimen and an approximately 45 mm x 45 mm area was captured around the crack tip. A light table was used for backlighting to get a clear view of the crack and interface and to avoid reflection and glare from the PMMA surface. Green colored paper was used between the surface of the light table and specimen to increase the visibility of cracks, and then the final pictures were formatted to black and white.

4.4 Experimental Observation and Results

4.4.1 Experimental observations for the low strength interfaces

For the weaker interfaces produced using the solvent based adhesive Weld-On 4, example experimental results showing the penetration/deflection behavior are illustrated in Figure 4-5(a)-Figure 4-5(d) for 90°, 85°, 80°, and 75°, respectively. The white vertical and nearly vertical lines are the interfaces, the horizontal lines on the left of the interfaces are the precracks, and horizontal or nearly horizontal lines on the right of the interfaces are the crack propagation. Discontinuities of the crack across the interface are denoted as deflection. Crack penetration is observed in Figure 4-5(a) and Figure 4-5 (b), while clear deflection is seen in Figure 4-5(c) and Figure 4-5 (d). In both Figure 4-5(c) and Figure 4-5 (d) the deflected crack eventually returns to

the mode I path causing final fracture of the specimens. Based on the results shown in Figure 4-5, it is clear the crack penetration/deflection transition is in the range of 80° – 85°.

More insight into the transition angle can be gained by observing each replicate test result near the transition. Clear penetration was observed for all the replicates at the 90° incident angle while clear deflection was observed at 80° and 75°. However, the replicates for 85° incident angle shows some ambiguity that is presented in Figure 4-6. While Figure 4-6 (a) has a clear horizontal line of penetration across the interface similar to that seen for the 90° samples, the penetrating crack in Figure 4-6 (b) has a lot of small branching. Similar branching is seen in Figure 4-6 (c) and Figure 4-6 (d) along with a small step at the interface. Such results suggest that 85° is very close to the transition between crack penetration and deflection for the lower strength interface samples.

4.4.2 Experimental observations for the high strength interfaces

The experimental results for the stronger interfaces created using Weld-On 16 are shown in Figure 4-7. Penetration is seen for incident angles 90° - 80° in Figure 4-7 (a)-(c), while deflection is observed in Figure 4-7 (d) for ϕ = 75°. Such results suggest the transition angle should reside in between 75° and 80°. While a clear straight line penetration is observed for incident angles of 90° and 85°, the penetration for the 80° samples shows some crack branching (Figure 4-7 (c)).

A closer look at all of the replicate results for an 80° incident angle bonded with Weld-On 16 show that they are not all clear penetration (Figure 4-8). While the crack penetrated straight across the interface in Figure 4-8 (a) and (b), in Figure 4-8 (c) and Figure 4-8 (d) the

penetrating crack does not run parallel to the precrack plane. The crack propagation direction is initially ~10° away from the precrack plane suggesting a small crack deflection likely deviated the penetrating crack path. Such results suggest that the transition angle is approximately 80° for the higher strength interface samples.

4.4.3 Comparison of experimental results with the energy based prediction method

In this study the toughness ratio, $\frac{\Gamma_I^s}{\Gamma^i}$, for each interface, i.e., the right side of the Eqn. 4.5 and Eqn. 4.6, have been determined experimentally. Considering the uncertainty of adhesion process of material, the average value of strength and toughness has been considered to calculate the average strength ratio and average toughness ratio in this study. The tested mechanical properties are shown in Table 4-2. The average toughness ratio for PMMA with Weld-On 4 is 1.24 and with Weld-On 16 is 1.22. The standard deviations of the two toughness ratios and strength ratios were estimated by the theory of propagation of uncertainty, which is provided in Table 3. Consider the measured toughness of PMMA with uncertainties $\Gamma_I^s \pm \mathrm{SD}(\Gamma_I^s)$ and interface (by Weld-On 4 or Weld-On 16) with uncertainties, $\Gamma^i \pm \mathrm{SD}(\Gamma^i)$. The uncertainty in the toughness ratio, using the theory of propagation of uncertainty, can be computed as $\mathrm{SD}(\frac{\Gamma_I^s}{\Gamma^i}) = \sqrt{(\frac{SD(\Gamma_I^s)}{\Gamma_I^s})^2 + (\frac{SD(\Gamma^i))}{\Gamma^i})^2}$. The uncertainties of the strength ratios $\mathrm{SD}(\frac{\hat{\sigma}_s}{\hat{\sigma}_i})$ were calculated in the similar way.

The corresponding critical incident angles for the deflection/penetration transition can be determined to be 37° based on the average toughness ratio. Lower and upper error bars were

calculated using ± one standard deviation from the mean value to be 0° ($\frac{\Gamma_I^s}{\Gamma^i}$= 0.94) and 52° ($\frac{\Gamma_I^s}{\Gamma^i}$= 1.5), respectively, for Weld-On 4. Similarly, the corresponding critical incident angles for the transition can be determined to be 36°, 16°, and 47° for average ($\frac{\Gamma_I^s}{\Gamma^i}$= 1.22), lower error bar ($\frac{\Gamma_I^s}{\Gamma^i}$= 1.04), and upper error bar ($\frac{\Gamma_I^s}{\Gamma^i}$= 1.4), respectively, for Weld-On 16 (Figure 4-9). In contrast, the experimental results in this study show the critical incident angles to be ~ 85° ± 2.5° and 80° ± 2.5° for Weld-On 4 and Weld-On 16, respectively. Thus, in the case of Weld-On 4 the energy based prediction of He and Hutchinson [50] underestimates critical incident angle by 56% of the experimental result, and 55% for Weld-On 16.

4.4.4 Comparison of experimental results with the cohesive zone model

Figure 4-10 has been adopted from Alam *et al.* [24] and was derived based on the CZM approach accounting for both the strength and toughness ratios. Figure 4-10 predicts that whether a crack will penetrate through, or deflect along, an interface depends not only on the toughness ratio and incident angle, but also on the strength ratio. The measured average strength and toughness ratios for PMMA bonded with Weld-On 4 are 4.1 and 1.24, respectively. It can be seen from Figure 4-10 that the corresponding critical incident angle is 76°, while the experimental observation is ~85°. The cohesive zone model underestimates the experimental result by only ~11 %. Considering the uncertainties, the critical angles for transition are ranging from 73° ($\frac{\hat{\sigma}_s}{\hat{\sigma}_i}$ - SD($\frac{\hat{\sigma}_s}{\hat{\sigma}_i}$) = 3.5 and $\frac{\Gamma_I^s}{\Gamma^i}$ - SD($\frac{\Gamma_I^s}{\Gamma^i}$) = 0.94) to 90° ($\frac{\hat{\sigma}_s}{\hat{\sigma}_i}$ + SD($\frac{\hat{\sigma}_s}{\hat{\sigma}_i}$) = 4.6 and $\frac{\Gamma_I^s}{\Gamma^i}$ + SD($\frac{\Gamma_I^s}{\Gamma^i}$) = 1.5) for Weld-On 4 Figure 4-10 (a).

Similarly, the measured average strength and toughness ratios for PMMA bonded with Weld-On 16 are 2.9 and 1.22, respectively. The predicted critical incident angle at the

deflection/penetration transition is found to be 68° from Figure 10, while the experimental observation is ~80°. In this case the cohesive zone model underestimates the experimental result by ~15 %. Analyzing the uncertainties, the range of the critical incident angle is found from 60° ($\frac{\hat{\sigma}_s}{\hat{\sigma}_i}$ - SD($\frac{\hat{\sigma}_s}{\hat{\sigma}_i}$) = 2.4, and $\frac{\Gamma_I^s}{\Gamma^i}$ - SD($\frac{\Gamma_I^s}{\Gamma^i}$) = 1.04) to 75° ($\frac{\hat{\sigma}_s}{\hat{\sigma}_i}$ + SD($\frac{\hat{\sigma}_s}{\hat{\sigma}_i}$) = 3.5, and $\frac{\Gamma_I^s}{\Gamma^i}$ + SD($\frac{\Gamma_I^s}{\Gamma^i}$) = 1.4) for Weld-On 16 Figure 4-10 (b).

4.5 Discussion

Predictions from two different types of methods, the energy-based method [50] and cohesive zone method (CZM) [24] have been compared with the experimental results in this study. This comparison has been visualized at Figure 4-11 and summarized at Table 4-3. While both methods underestimate incident angle at transition, and predictions by CZM are much closer to the experimental results than those using the energy-based method.

CZM considers both the toughness and strength ratios, whereas the energy-based method considers only the toughness ratio. It was the intent of this study to choose interfaces that had exactly the same toughness, however, significantly different strengths. It is challenging to find materials to make the perfectly desired interfaces. The two selected interfaces in this experimental study had similar, although not exactly same, toughness ratios with a small difference magnitude of ~2%. In contrast the difference in the strength ratios was much more significant at 41%. Furthermore, the use of solvent bonding methods chemically joins the PMMA without introducing a layer of dissimilar polymer that with unique elastic properties that affect the crack tip stress field and local strain energy release rate. So while no experimental interface is likely perfect for this study, the chosen model material system appears to be a good one.

The CZM model predicts the critical transition angle to be ~8° higher for the weaker PMMA interface, while the energy-based approach predicts only ~2° higher. While a 2° difference should be undetectable by the present experiments, an 8° difference should be easily detected by using 5° increments in incident angle. The experimental results suggest the actual difference in critical angle is between 5° and 10° and thus is in good agreement with the CZM model. Overlooking the required stress for creating stress field at the crack tip during transition by the energy-based method lead to the underestimation of the experimental results.

Finally, the published strength-based approaches that make predictions based solely on the strength ratios, such as those by [16] and [28], focus only on 90° incident angles are were unsuitable for the above comparisons of the critical incident angle. However, one can compare the present results to the strength-based predictions by using only the 90° incident angle experiments. [16] predicted that for a 90° incident angle the crack should deflect for a substrate-to-interface strength ratio equal to or greater than 3.5. Based on the strength ratios given in Table 4-3, this model predicts that the weaker interfaces in this study should have deflected the crack for the 90° incident angle case, while the stronger interfaces should have promoted crack penetration at 90°. In contrast, the experimental results revealed penetration for both types of interfaces with a 90° incident angle, which clearly disagrees with their prediction. However, the experimental results don't disagree with the prediction by [28], where the critical strength ratio was estimated to be approximately at 5.0. Unfortunately, strength ratios greater than 5.0 were not achieved using the present model material system and such work is left to future studies.

4.6 Conclusion

Based on an experimental study comparing different methods for predicting the crack deflection/penetration transition of a crack incident to an interface, the following conclusions can be made:

- Although both the cohesive zone model (CZM) and energy-based approaches underestimate the incident angle at transition, the CZM predictions are much closer to the experimental results.
- The effect of the strength ratio on the penetration/deflection behavior is significant along with the toughness ratio. Using only the toughness ratio, and thereby ignoring the strength ratio, provides a severe underestimation of the critical angle for the crack penetration/deflection transition.
- The strength-based approach of Gupta et *al.* [16] was not able to correctly predict the observed crack penetration behavior for a 90° incident angle, while the approach of Cook et *al.* [28] could not be tested using the present model material system.

Table 4-1: Material properties of the Acrylic Sheet.

Property	
Density (kg/m3)	1190
Young's modulus (GPa)	2.8
Poisson's ratio	0.37
Color	Colorless

Table 4-2: Measured properties of the interfaces used in this study.

Adhesive	Tensile strength (MPa)			Fracture Toughness (J/m^2)		
	Average	Standard deviation	Number of repetitions	Average	Standard deviation	Number of repetitions
PMMA	66.5	1.9	5	679.7	75.8	10
Weld-On 4	16.2	2.1	5	548.5	115.1	3
Weld-On 16	22.6	4.0	5	557.2	56.7	3

Table 4-3: Prediction of energy based method and cohesive zone model.

Interfaces	Toughness ratio $(\frac{\Gamma_I^s}{\Gamma^i})$		Strength ratio $(\frac{\hat{\sigma}_s}{\hat{\sigma}_i})$		Experimental Observation		Predicted by Energy-based method		Predicted Cohesive zone model	
	Average	St. deviation	Average	St. deviation	Critical angle	Replicates number	Critical angle	Deviation from experimental observation	Critical angle	Deviation from experimental observation
Weld-On 4	1.24	0.29	4.1	0.55	~85°	4	37°	56%	76°	11%
Weld-On 16	1.22	0.18	2.9	0.53	~80°	4	36°	55%	68°	15%

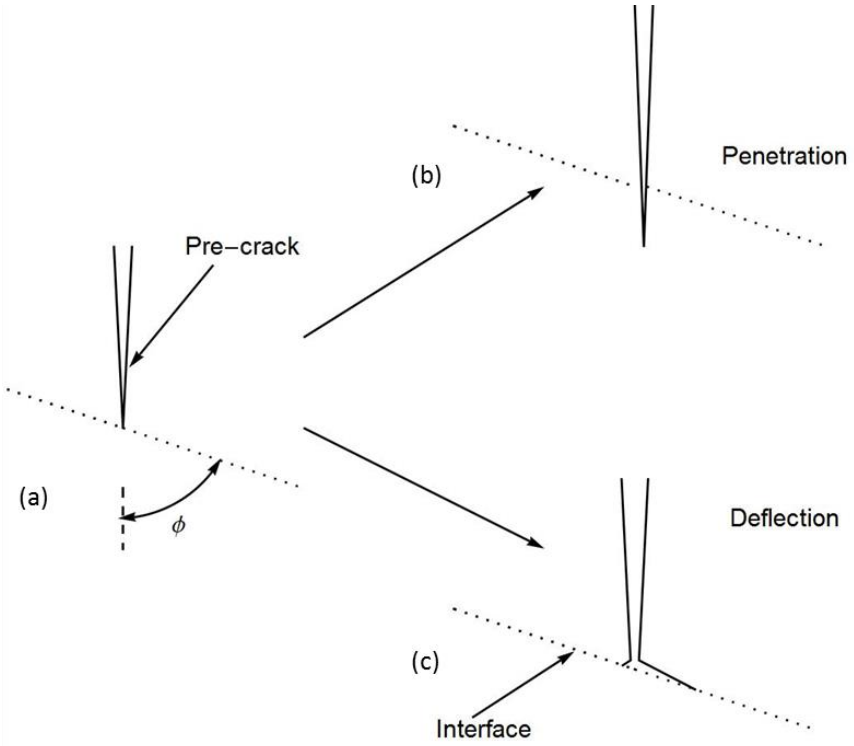

Figure 4-1: Schematic of (a) a crack incident on an interface with an incident angle ϕ, and two potential directions of crack-propagation shown in (b)-(c).

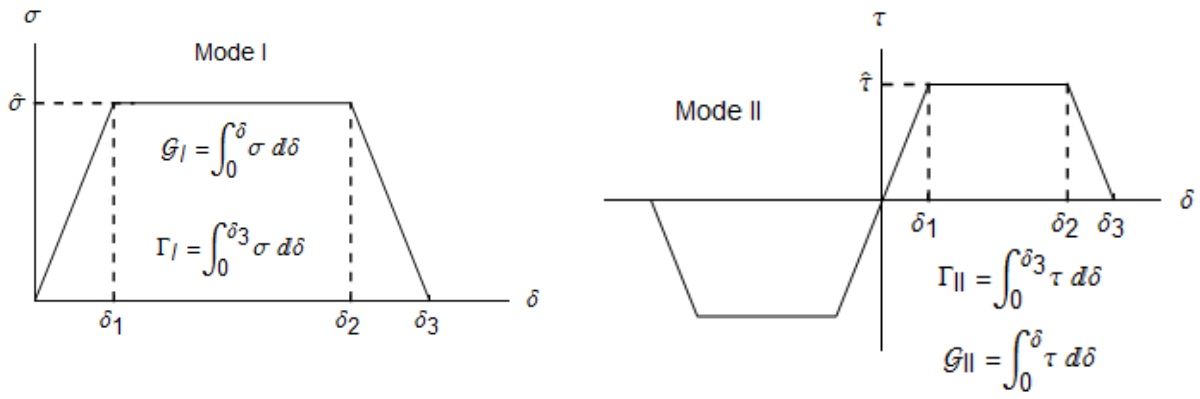

Figure 4-2: Trapezoidal traction-separation laws for cohesive zone model.

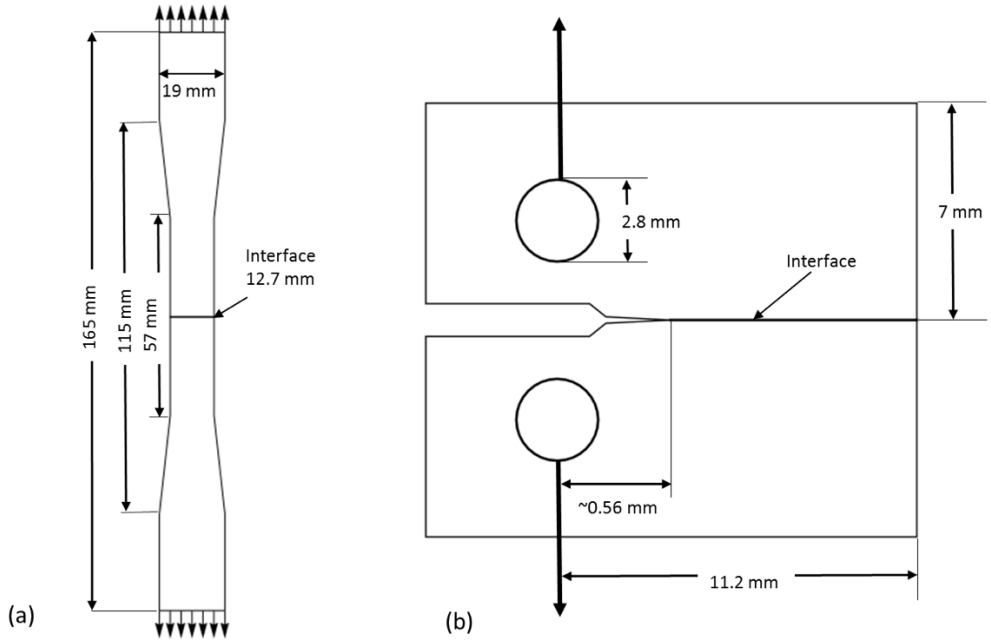

Figure 4-3: Nonstandard: (a) tensile test specimen for adhesive strength testing and (b) compact test specimen for toughness testing.

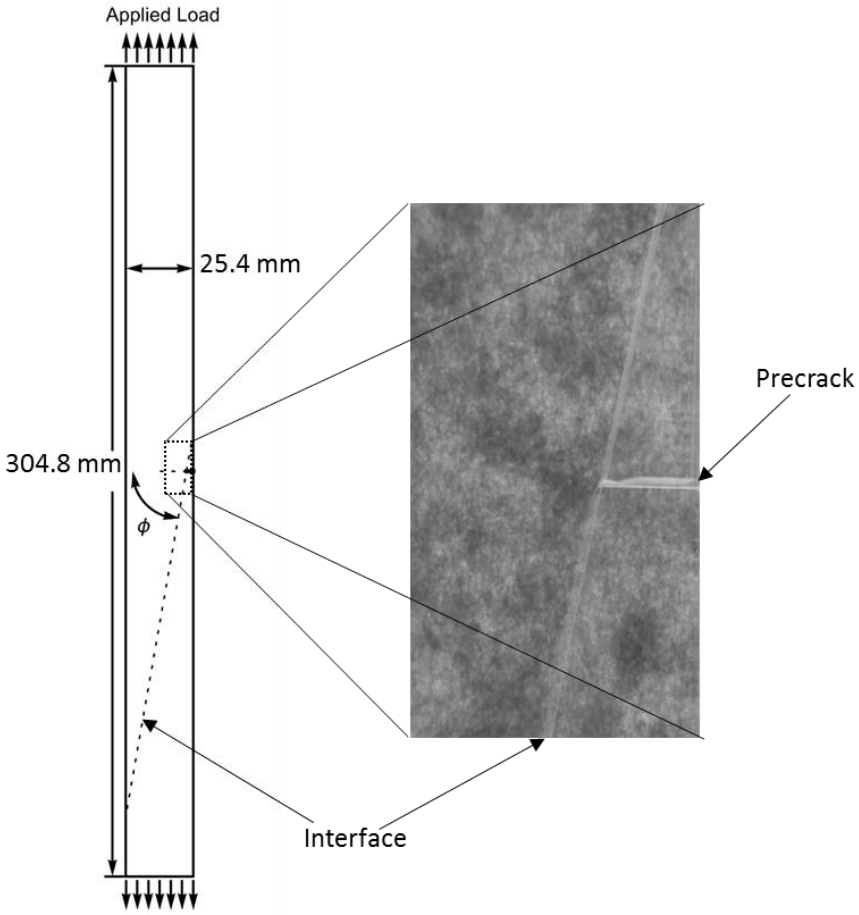

Figure 4-4: Schematic of the specimen studied, where the length of precrack is 2.54 mm. The magnified picture is the region of interest in this study.

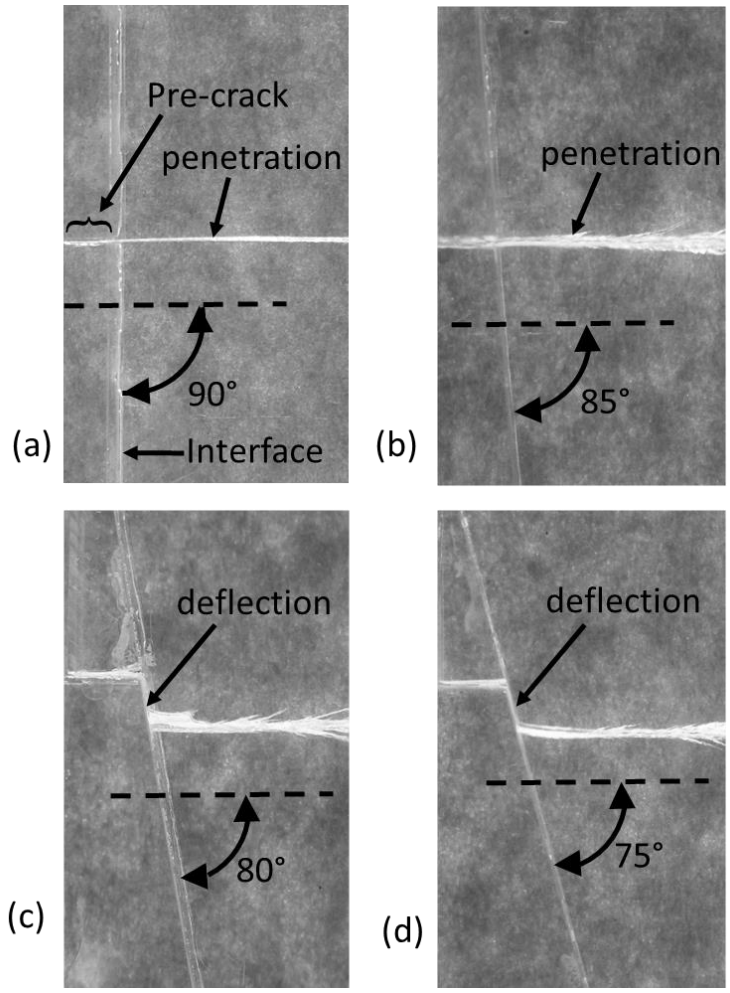

Figure 4-5: Experimental observations for weaker interface by Weld-On 4. Incident angle decreases for 5° on every picture from (a)-(d) for 90° to 75° respectively.

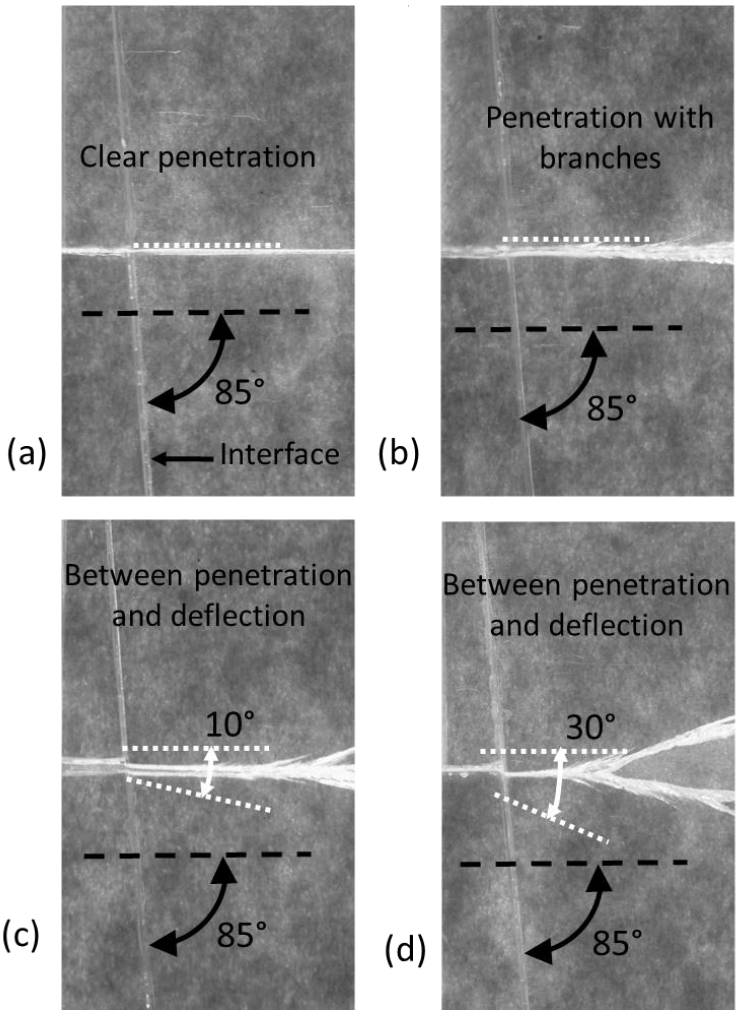

Figure 4-6: Replicates for 85° incident angle of Weld-On-4 that shows the ambiguity between deflection and penetration. White dotted lines and angles shows the deviation of crack penetration direction from horizontal penetration.

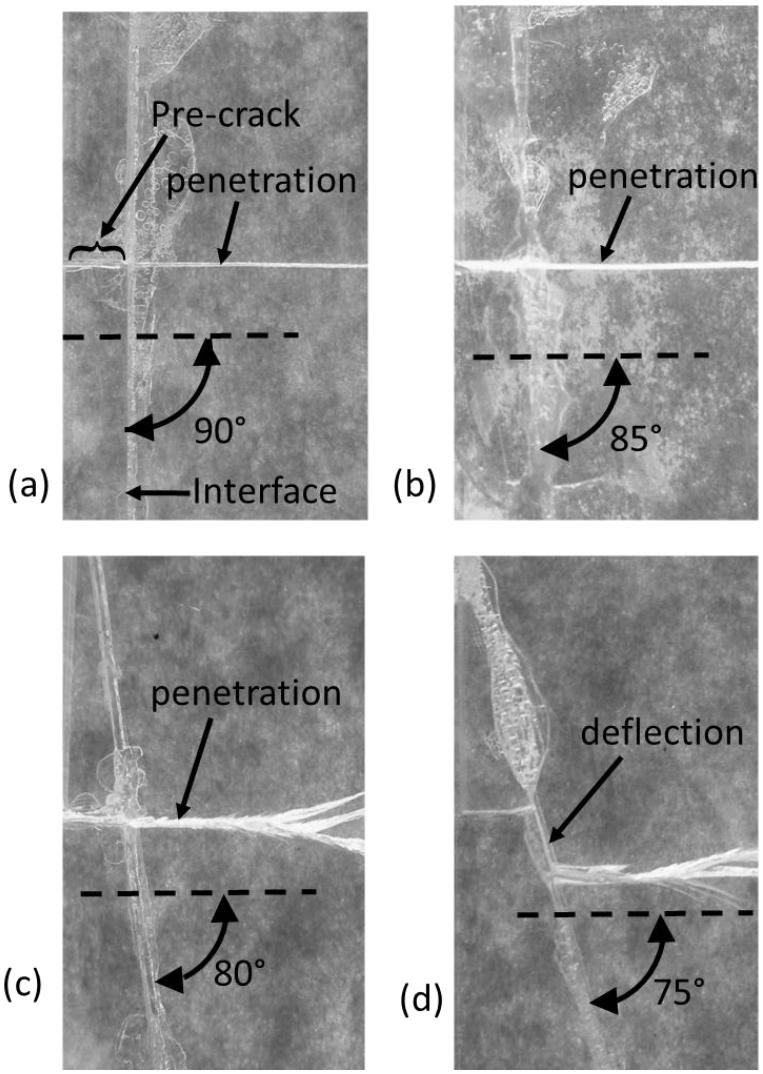

Figure 4-7: Experimental results for stronger interfaces by Weld-On 16. Incident angle decreases for 5° on every picture from (a)-(d) for 90° to 75° respectively.

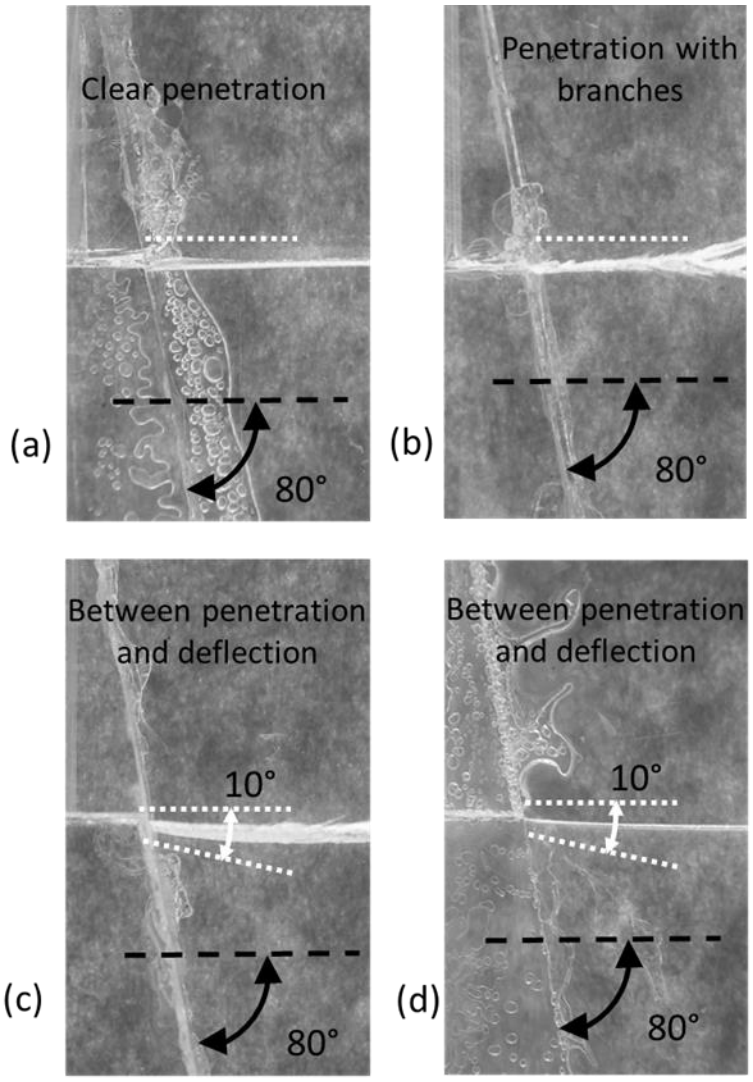

Figure 4-8: Replicates for 80° incident angle of Weld-On 16 that shows the ambiguity between deflection and penetration.

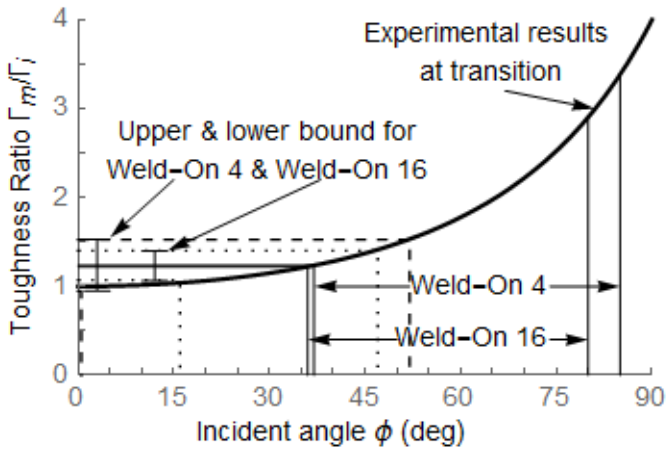

Figure 4-9: Toughness ratio at transition as a function of incident angle ϕ. Points falling in the area below of the curve are predicted to give interface penetration, while those points in the area above the curve are predicted to give interface deflection. The large deviation between the predictions and the experimental results are shown.

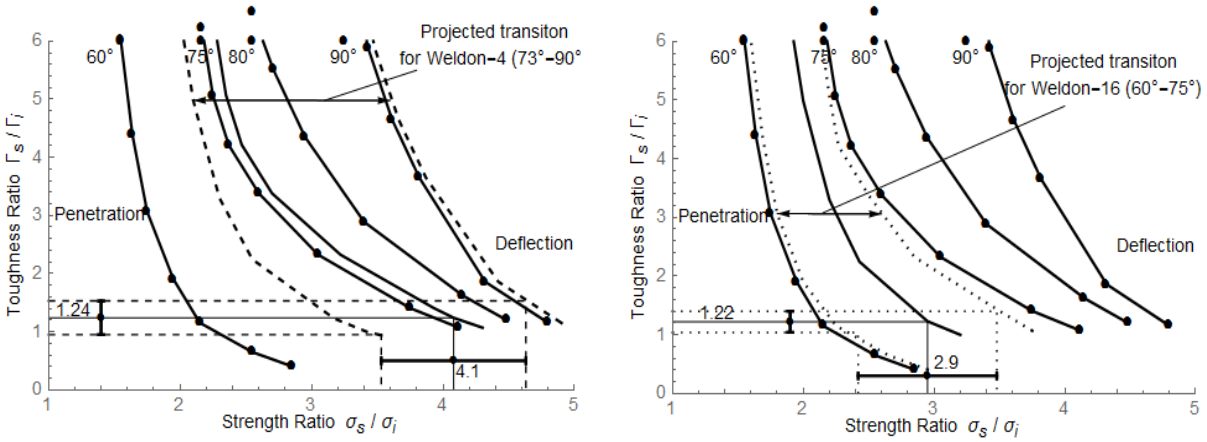

Figure 4-10: Cohesive zone model based prediction adopted from Alam et *al.* [24]. The solid lines represent the transition between penetration and deflection for various incident angles which each data point showing where the calculations were conducted. (a) The dashed line characterizes the projected upper and lower error bar for one standard deviation of transition

angles for the interface by Weld-On 4, and (b) the dotted line showed the upper and lower error bar for Weld-On 16.

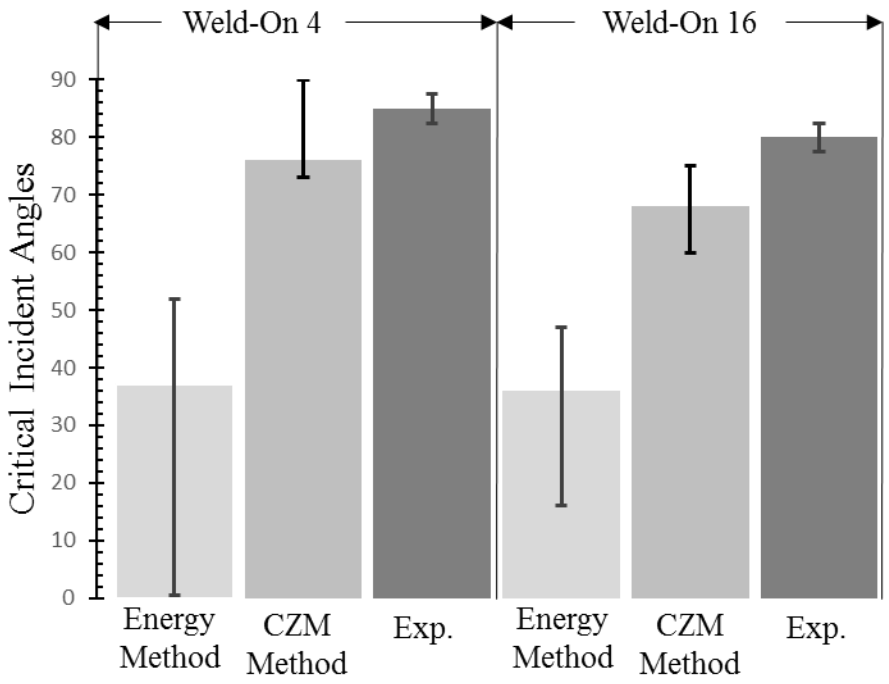

Figure 4-11: Bar graph from left to right for Weld-On 4 and Weld-On 16 are illustrated: i) the predictions by energy-based method, ii) Cohesive-zone method, and iii) experimental observation. Error bar due to standard deviation from the mean prediction is provided.

Chapter 5 : General Conclusion

The computational study of this dissertation work revealed the un-exposed potentiality of stress-and-energy base approach cohesive-zone method, and the experimental study checked the accuracy of predicting crack deflection by different approaches. Commercially available finite element solver, Abaqus, along with Fortran user-defined element (UEL) used in this model. A trapezoidal shaped traction law used to define the properties of cohesive-zone materials. Dimensionless parameters used as generalized material properties. A simple circular geometry at crack-tip was chosen to represent single-edge-notch specimen under tensile load. This computational analysis composed of two studies.

The first computational study evaluated the effect of incident angle on crack deflection. The effect of dimensionless parameters: fracture-length scale, and normalized-toughness were investigated. It showed the presence of K-field at the crack-tip for small fracture-length scales, and the absence of K-field for larger fracture-length scales. Deflection is more likely for low strength, low toughness and small incident angles. The decreasing incident angles becomes more strength ratio dependent and at zero-degree incident angle it is completely strength-ratio dependent. Transition at large incident angles are more sensitive than small incident angles. The effect of normalized-toughness is very low and LEFM solution recovered at zero-degree incident angle case.

The second study examined the interfacial stress state mechanism during transition between penetration and deflection for quasi-static tensile loading using cohesive-zone model. This study used the same circular model and boundary conditions as the previous study. It appeared that only mode-I stress field exists at penetration, while mode-I and mode-II acts simultaneously at transition or deflection. The existence of smaller phase angle has been shown during transition than the phase angle at deflection. Examining the effect of fracture-length scales it appeared that the phase angle at transition increases as interface and materials fracture-length scales decreases. The phase angle results at transition meet LEFM solutions at small fracture-length scales. Normalized-toughness illustrated a smaller effect on the stress states at an interface for large equal fracture-length scales while the effect is larger at small equal fracture length scales. Finally, the

effect of modulus mismatch was examined and it was noted that stiffer cracked layer provides higher mixed-modeness at interfaces during transition.

Finally, an experimental study was performed to compare the experimental observations with the prediction of crack deflection by cohesive-zone method, energy-based LEFM, and strength-based methods. It was shown that cohesive-zone model can predict crack deflection better than energy-based LEFM. Two popular strength based methods were compared and one of them [16] cannot correctly predict deflection, another method [28] was not possible to test using our current set of material systems. It appeared that both the interface-to-substrate strength ratio have strong influence on crack penetration/deflection behavior. This work explained a method for characterizing transition events between penetration and deflection. The significance of this study is that the results of this work will help designers to choose the right criteria for predicting crack deflection. The results of this analysis also provide a bench-mark for future computational modeling.

Chapter 6: Bibliography

[1] Bao G, Suo Z. Remarks on Crack-Bridging Concepts. Applied Mechanics Reviews. 1992;45:355-66.

[2] He MY, Heredia FE, Wissuchek DJ, Shaw MC, Evans AG. The mechanics of crack growth in layered materials. Acta Metallurgica et Materialia. 1993;41:1223-8.

[3] Spearing SM, Evans AG. The role of fiber bridging in the delamination resistance of fiber-reinforced composites. Acta Metallurgica et Materialia. 1992;40:2191-9.

[4] Parmigiani JP. Delamination and deflection at interfaces. Ann Arbor: University of Michigan; 2007.

[5] Evans AG, Marshall DB. Overview no. 85 The mechanical behavior of ceramic matrix composites. Acta Metallurgica. 1989;37:2567-83.

[6] Campbell GH, Rühle M, Dalgleish BJ, Evans AG. Whisker Toughening: A Comparison Between Aluminum Oxide and Silicon Nitride Toughened with Silicon Carbide. Journal of the American Ceramic Society. 1990;73:521-30.

[7] Koester KJ, Ager JW, Ritchie RO. The true toughness of human cortical bone measured with realistically short cracks. Nat Mater. 2008;7:672-7.

[8] Wang R, Gupta HS. Deformation and Fracture Mechanisms of Bone and Nacre. Annual Review of Materials Research. 2011;41:41-73.

[9] Zimmermann EA, Launey ME, Ritchie RO. The significance of crack-resistance curves to the mixed-mode fracture toughness of human cortical bone. Biomaterials. 2010;31:5297-305.

[10] Jones DR, Ashby MF. Engineering materials 2: an introduction to microstructures, processing and design. Woburn, MA: Butterworth-Heinemann; 2005.

[11] Termine JD, Kleinman HK, Whitson SW, Conn KM, McGarvey ML, Martin GR. Osteonectin, a bone-specific protein linking mineral to collagen. Cell. 1981;26:99-105.

[12] Yan J, Mecholsky Jr JJ, Clifton KB. How tough is bone? Application of elastic–plastic fracture mechanics to bone. Bone. 2007;40:479-84.

[13] Becher PF, Sun EY, Hsueh C-H, Alexander KB, Hwang S-L, Waters SB, et al. Debonding of interfaces between beta-silicon nitride whiskers and Si□Al□Y oxynitride glasses. Acta Materialia. 1996;44:3881-93.

[14] Foulk IJW, Johnson GC, Klein PA, Ritchie RO. On the toughening of brittle materials by grain bridging: Promoting intergranular fracture through grain angle, strength, and toughness. Journal of the Mechanics and Physics of Solids. 2008;56:2381-400.

[15] Inglis CE. Stresses in a plate due to the presence of cracks and sharp corners. the Institute of Naval Architects1913. p. 219-30.

[16] Gupta V, Argon AS, Suo Z. Crack Deflection at an Interface Between Two Orthotopic Media. Journal of Applied Mechanics. 1992;59:S79-S87.

[17] Ming-Yuan H, Hutchinson JW. Crack deflection at an interface between dissimilar elastic materials. International Journal of Solids and Structures. 1989;25:1053-67.

[18] Hutchinson JW, Suo Z. Mixed mode cracking in layered materials. Advances in applied mechanics. 1991;29:63-191.

[19] He MY, Evans AG, Hutchinson JW. Crack deflection at an interface between dissimilar elastic materials: Role of residual stresses. International Journal of Solids and Structures. 1994;31:3443-55.

[20] Griflith A. The phenomenon of rupture and flow in solids. Phil Trans Roy Soc. London1920. p. 163-98.

[21] Parmigiani JP, Thouless MD. The roles of toughness and cohesive strength on crack deflection at interfaces. Journal of the Mechanics and Physics of Solids. 2006;54:266-87.

[22] Parmigiani JP, Thouless MD. The effects of cohesive strength and toughness on mixed-mode delamination of beam-like geometries. Engineering Fracture Mechanics. 2007;74:2675-99.

[23] Strom JL, Parmigiani JP. Transition of crack path at bi-material interfaces. Engineering Fracture Mechanics. 2014;115:13-21.

[24] Alam M, Grimm B, Parmigiani JP. Effect of incident angle on crack propagation at interfaces. Engineering Fracture Mechanics. 2016;162:155-63.

[25] Kafkalidis MS, Thouless MD, Yang QD, Ward SM. Deformation and fracture of adhesive layers constrained by plastically-deforming adherends. Journal of Adhesion Science and Technology. 2000;14:1593-607.

[26] Xu LR, Huang YY, Rosakis AJ. Dynamic crack deflection and penetration at interfaces in homogeneous materials: experimental studies and model predictions. Journal of the Mechanics and Physics of Solids. 2003;51:461-86.

[27] Rosakis A, Xia K, Lykotrafitis G, Kanamori H. Dynamic shear rupture in frictional interfaces: speeds, directionality, and modes: Elsevier; 2015.

[28] Cook J, Gordon JE, Evans CC, Marsh DM. A Mechanism for the Control of Crack Propagation in All-Brittle Systems. Proceedings of the Royal Society of London Series A Mathematical and Physical Sciences. 1964;282:508.

[29] Lu M-C, Erdogan F. Stress intensity factors in two bonded elastic layers containing cracks perpendicular to and on the interface. I Analysis. II-Solution and results. 1983.

[30] Martínez D, Gupta V. Energy criterion for crack deflection at an interface between two orthotropic media. Journal of the Mechanics and Physics of Solids. 1994;42:1247-71.

[31] Tullock DL, Reimanis IE, Graham AL, Petrovic JJ. Deflection and penetration of cracks at an interface between two dissimilar materials. Acta Metallurgica et Materialia. 1994;42:3245-52.

[32] Liu LG, Ou ZC, Duan ZP, Pi AG, Huang FL. Strain-rate effects on deflection/penetration of crack terminating perpendicular to bimaterial interface under dynamic loadings. International Journal of Fracture. 2011;167:135-45.

[33] Martin E, Poitou B, Leguillon D, Gatt JM. Competition between deflection and penetration at an interface in the vicinity of a main crack. International Journal of Fracture. 2008;151:247-68.

[34] Kafkalidis MS, Thouless MD. The effects of geometry and material properties on the fracture of single lap-shear joints. International Journal of Solids and Structures. 2002;39:4367-83.

[35] Li S, Thouless MD, Waas AM, Schroeder JA, Zavattieri PD. Mixed-mode cohesive-zone models for fracture of an adhesively bonded polymer–matrix composite. Engineering Fracture Mechanics. 2006;73:64-78.

[36] Yang QD, Thouless MD. Mixed-mode fracture analyses of plastically-deforming adhesive joints. International Journal of Fracture. 2001;110:175-87.

[37] Metcalf J, Kobayashi T. Comparison of crack behavior in Homalite 100 and Araldite B. In: Kanninen GTHaMF, editor. Crack Arrest Methodology and Applications. Philadelphia: ASTM International; 1980. p. 128-45.

[38] Dowling NE. Mechanical behavior of materials: engineering methods for deformation, fracture, and fatigue. 2nd ed: Prentice hall; 1999.

[39] Parmigiani JP. Delamination and deflection at interfaces: University of Michigan; 2007.

[40] Wilson WK, Cherepko J. Analysis of cracks with multiple branches. International Journal of Fracture. 1983;22:303-15.

[41] Cook RF. Segregation effects in the fracture of brittle materials: Ca□Al2O3. Acta Metallurgica et Materialia. 1990;38:1083-100.

[42] Khan A, Chan HM, Harmer MP, Cook RF. Toughening of an Alumina—Mullite Composite by Unbroken Bridging Elements. Journal of the American Ceramic Society. 2000;83:833-40.

[43] Tu W-C, Lange FF, Evans AG. Concept for a Damage-Tolerant Ceramic Composite with "Strong" Interfaces. Journal of the American Ceramic Society. 1996;79:417-24.

[44] Inglis CE. Stresses in a plate due to the presence of cracks and sharp corners. the Institute of Naval Architects1913. p. 219-30.

[45] Williams M, Zak A. Crack point stress singularities at a bi-material interface. California Institute of Technology; 1962. p. 142-3.

[46] Rice JR. Elastic Fracture Mechanics Concepts for Interfacial Cracks. Journal of Applied Mechanics. 1988;55:98-103.

[47] Griffith A. The phenomenon of rupture and flow in solids. Phil Trans Roy Soc. London1920. p. 163-98.

[48] Irwin GR. Analysis of stresses and strains near the end of a crack traversing a plate. Journal of Applied Mechanics. 1957:361-4.

[49] Orowan E. Fracture and strength of solids. Reports on Progress in Physics. 1949;12:185.

[50] He M-Y, Hutchinson JW. Crack deflection at an interface between dissimilar elastic materials. International Journal of Solids and Structures. 1989;25:1053-67.

[51] Hutchinson JW, Suo Z. Mixed Mode Cracking in Layered Materials. In: John WH, Theodore YW, editors. Advances in Applied Mechanics: Elsevier; 1991. p. 63-191.

[52] Cotterell B, Rice JR. Slightly curved or kinked cracks. International Journal of Fracture. 1980;16:155-69.

[53] Barenblatt GI. The Mathematical Theory of Equilibrium Cracks in Brittle Fracture. In: H.L. Dryden TvKGKFHvdD, Howarth L, editors. Advances in Applied Mechanics: Elsevier; 1962. p. 55-129.

[54] Dugdale DS. Yielding of steel sheets containing slits. Journal of the Mechanics and Physics of Solids. 1960;8:100-4.

[55] Alam M, Parmigiani JP. Crack propagation at bi-material interfaces. PAMM. 2015;15:143-4.

[56] Wang H, Lu W, Barber JR, Thouless MD. The roles of cohesive strength and toughness for crack growth in visco-elastic and creeping materials. Engineering Fracture Mechanics. 2016;160:226-37.

[57] Anderson TL. Fracture mechanics: fundamentals and applications: CRC press; 2005.

[58] Roy Xu L, Y. Huang Y, Rosakis AJ. Dynamic crack deflection and penetration at interfaces in homogeneous materials: experimental studies and model predictions. Journal of the Mechanics and Physics of Solids. 2003;51:461-86.

[59] Rosakis AJ, Ravichandran G. Dynamic failure mechanics. International Journal of Solids and Structures. 2000;37:331-48.

[60] Maccagno TM, Knott JF. The fracture behaviour of PMMA in mixed modes I and II. Engineering Fracture Mechanics. 1989;34:65-86.

[61] Sundaram BM, Tippur HV. Dynamics of crack penetration vs. branching at a weak interface: An experimental study. Journal of the Mechanics and Physics of Solids. 2016;96:312-32.

[62] Krishnan A, Xu LR. Systematic Evaluation of Bonding Strengths and Fracture Toughnesses of Adhesive Joints. The Journal of Adhesion. 2011;87:53-71.